Master's thesis

NTNU
Norwegian University of Science and Technology
Faculty of Medicine and Health Sciences
Department of Clinical and Molecular Medicine

Konstanse Skogøy Innvær

The role of TDG-mediated DNA demethylation in the entorhinal-hippocampal spatial representation system

Master's thesis in Molecular Medicine
Supervisor: Jing Ye
Co-supervisor: Magnar Bjørås
May 2022

NTNU
Kunnskap for en bedre verden

Konstanse Skogøy Innvær

The role of TDG-mediated DNA demethylation in the entorhinal-hippocampal spatial representation system

Master's thesis in Molecular Medicine
Supervisor: Jing Ye
Co-supervisor: Magnar Bjørås
May 2022

Norwegian University of Science and Technology
Faculty of Medicine and Health Sciences
Department of Clinical and Molecular Medicine

NTNU
Norwegian University of
Science and Technology

Abstract

Cognitive impairments and memory decline are commonly seen with aging. The decline is often seen with epigenetic alterations, such as in DNA methylation and demethylation. Studies on 5-hydroxymethylcytosine (5hmC) levels during development have been performed, but there are few considering altered DNA demethylation intermediate levels during aging. By investigating TDG-mediated DNA demethylation during aging in the entorhinal and hippocampal region, we can get an insight in whether DNA demethylation is an important molecular mechanism underlying age-dependent cognitive impairments.

In this study, the first aim is to investigate whether DNA demethylation intermediates are accumulated during aging. I assess the level of 5-formylcytosine (5fC) and 5-carboxylcytosine (5CaC) in the medial entorhinal cortex (MEC) and in the hippocampus (HPC) of young (3 months old) and aged (18 months old) mice by Immunohistochemistry (IHC) and confocal microscopy. Confocal images were analyzed in 3D by IMARIS Cell imaging software, and the statistical analysis was performed in GraphPad Prism. I found that levels of 5fC and 5CaC were significantly increased in aged MEC and CA1 when compared to young, indicating that both 5fC and 5CaC are accumulated in MEC and HPC during aging.

As these DNA demethylation intermediates (5fC and 5CaC) are excised by thymine DNA glycosylase (TDG)-mediated DNA base excision repair (BER) pathway, the second aim of this study is to establish a reliable method for the conditional manipulation of TDG expression in neurons using the Cre-loxP system. For this purpose, I assess rAAV-Cre induced TDG-depletion in the hippocampal region of *LoxP-MiniTdg*$^{+/+}$ mice by IHC. Antibodies specific for GFP and markers of mature neurons, astrocytes and microglia were used in this study. I found that injection of the rAAV-Cre viral stock with a dilution of 1:5 and 1:10 led to neuronal loss along with an escalation of activated GFAP-positive astrocytes and Iba1-positive microglia. Injection of the rAAV-Cre viral stock with a dilution of 1:20 showed nice Cre-induced GFP expression in both pyramidal and granular cell layers, with limited neuronal loss and immune response. In addition, RT-qPCR was performed to evaluate the TDG-levels after depletion, but only a pilot experiment was performed. I did not get any reliable results showing TDG depletion due to limited sample size.

Taken together, my work suggests that (i) DNA methylation intermediates such as 5fC and 5CaC were accumulated in MEC and HPC neurons during aging; (ii) 1:20 rAAV-Cre injection ensures the most efficient TDG depletion in the hippocampal region without introducing other side effects such as tissue lesions and immune response.

Sammendrag

Hukommelsestap og kognitive svekkelser er ofte sett med aldring. Degenerasjonen sees ofte i sammenheng med epigenetisk endring, som i DNA metylering og demetylering. Flere studier som omhandler 5-hydroxymethylcytosine (5hmC) nivå under utvikling er blitt utført, men få er gjort i sammenheng med nivåer av mellomprodukter fra DNA demetylering ved aldring. Ved å undersøke TDG-mediert DNA metylering ved aldring i entorhinal cortex og hippocampus kan vi få et innblikk i om DNA demetylering er en viktig molekylær mekanisme som ligger til grunn for aldersavhengige kognitive svikt.

Det første målet i dette studie er å undersøke om nivå av mellomprodukter fra DNA demetylering akkumuleres ved aldring. Jeg vurderer nivået av 5-formylcytosin (5fC) og 5-karboxylcytosin (5CaC) i mediale entorhinal cortex (MEC) og i hippocampus (HPC) til unge (3 måneder gamle) og eldre (18 måneder gamle) mus ved hjelp av immunhistokjemi (IHC) og konfokal mikroskopi. 3D analyse av konfokale bilder ble utført i programvaren IMARIS. Jeg fant en signifikant økning av 5fC og 5CaC nivåer i eldre MEC og CA1, sammenlignet med unge, som indikerer at både 5fC og 5CaC akkumuleres i MEC og HPC ved aldring.

Ettersom mellomproduktene fra DNA demetylering (5fC og 5CaC) blir fjernet av tymin-DNA-glykosylase (TDG) mediert eksisjonsreparasjon (BER), er det andre målet med studiet å etablere en pålitelig metode for manipulering av TDG uttrykkelse i nevroner, ved å bruke Cre-loxP systemet. For dette formålet evaluerer jeg rAAV-Cre-indusert fjerning av TDG i hippocampus regionene til *LoxP-MiniTdg* $^{+/+}$ mus ved hjelp av IHC. Antistoffene som ble brukt er spesifikke for GFP, modne nevroner, astrocytter og mikroglia. Jeg oppdaget at rAAV-Cre viral injeksjoner med 1:5 og 1:10 fortynning førte til tap av nevroner i sammenheng med eskalert aktivering av GFAP-positive astrocytter og Iba1-positive mikroglia. Injeksjoner av rAAV-Cre virus med en fortynning på 1:20 viste jevn uttrykkelse av Cre-indusert GFP i både pyramidale og granulære cellelag, med begrenset tap av nevroner og immunrespons. I tillegg ble RT-qPCR utført for å evaluere TDG-nivåene etter rAAV-Cre injeksjoner, men kun et pilotforsøk ble utført. Jeg fikk ingen pålitelige resultater som viser mangel av TDG på grunn av begrenset antall prøver.

Til oppsummering antydet arbeidet mitt at (i) Mellomprodukter av DNA demetylering, som 5fC og 5CaC, ble akkumulert i nevroner i MEC og HPC ved aldring; (ii) 1:20 rAAV-Cre injeksjon sikrer den mest effektive fjerningen av TDG i hippocampus regionen ute å introdusere andre bivirkninger som vevslesjoner og immunrespons.

Acknowledgments

To begin, I would like to thank my supervisor, Jing Ye, who guided me through writing my thesis with always being available for discussions and by giving me advice along the way. I would also like to thank my co-supervisor, Magnar Bjørås, for giving me the opportunity to write my thesis at the Institute of Clinical and Molecular Medicine (IKOM) at the Norwegian University of Science and Technology. Special thanks to the members of the Research Team that always helped when I needed assistance or advice: Marion Fernandez who mentored me and trained me in laboratory methods, Anna Bugaj who helped me with analytical approaches, Dagny Døskeland who did the *in vivo* part of my thesis and contributed to the collection of data, Mina Heggedal who shared my workload when time ran short and who was always up for thesis related discussions, and Vidar Saasen who assisted me with general laboratory issues. I would also like to thank the rest of laboratory members from different research teams that made me feel welcome at the laboratory and helped me whenever I had any questions. Finally, I would like to thank family and friends who always have believed in me, supported me, and motivated me through all my years as a student.

Table of Content

Abbreviations

Abbreviations	Meaning
AD	Alzheimer's disease
AP	Abasic
BER	Base excision repair
CA	Cornu ammonis
CNS	Central nervous system
CREB1	cAMP-response-element-binding protein 1
CT	Cycle threshold
DG	Dentate gyrus
DMP	DNA methylation program
DNMT1	DNA methyltransferase 1 (Maintenance)
DNMT3a/3b	DNA methyltransferase 3a/3b (*de novo*)
EC	Entorhinal cortex
FC	Fold change
GFAP	Glial fibrillary acidic protein
GFP	Green fluorescent protein
HPC	Hippocampus
IHC	Immunohistochemistry
LTP	Long-term potentiation
MEC	Medial entorhinal cortex
MTL	Medial temporal lobe
PFA	Paraformaldehyde
rAAV	Recombinant Adeno Associated Virus
SAM	S-adenosyl methionine
TDG	Thymine-DNA glycosylase
TET	Ten-eleven translocase
WT	Wild type
5CaC	5-carboxylcytosine
5fC	5-formylcytosine
5mC	5-methylcytosine
5hmC	5-hydroxymethylcytosine

List of figures and tables

1. Introduction

1.1 Epigenetics

Epigenetics are characterized as changes in gene expression, while the DNA sequence remains unaltered [1]. The major mechanisms of epigenetics are DNA methylation, histone modification, and non-coding RNA targeting [2]. In general, epigenetic modifications activate or repress gene transcription through a myriad of processes that alters chromatin structure to either compact heterochromatin or to a loosely packed euchromatin [2, 3]. To achieve the correct chromatin structure, enzymes known as writers, readers, and erasers, function as chemical regulators. Writers modify histone tails or DNA, erasers remove the modifications, while readers communicate with the set epigenetic modifications and impact chromatin structure through recruitment of transcription- and remodeling factors [3]. The chromatin remodeling either inhibits or allows transcriptional factors to bind to regulatory genomic areas. If the neuronal functions are epigenetically modified, it might impact learning and memory, making epigenetic regulation in the brain crucial [4-6]. In the following sections, DNA methylation and demethylation will be in focus.

1.1.1 DNA methylation

DNA methylation is when a methyl group is covalently added to the 5´position of cytosines on DNA strands, and 5-methylcytosine (5mC) is produced [7]. The process occurs in both promoter regions and gene bodies in CpG islands, which are genomic regions with a generous amount of CpG dinucleotides. Depending on the methyl group location, DNA methylation transcriptionally regulates gene expression. DNA methylation in promoter regions inhibits transcription, as the methyl group alters the formation of the DNA, preventing transcription factors to recognize their binding site [4, 7, 8]. At the same time, upregulated gene transcription has been observed in association with methylated CpG regions in gene bodies [7-9]. The formation of 5mC is catalyzed by DNA methyltransferases (DNMTs), that transfer methyl groups donated by S-adenyl methionine (SAM) [6, 9]. DNMT1, known as the maintenance methyltransferase, mediates the methylation of hemimethylated daughter strands during DNA replications and ensures that the methylation patterns from the parental DNA strand are maintained (Figure 1A) [6, 7]. On the other hand, DNMT3A and 3B are responsible for *de novo* methylations, where methyl groups are added to unmethylated cytosines, creating a new methylation pattern (Figure 1B) [6, 8].

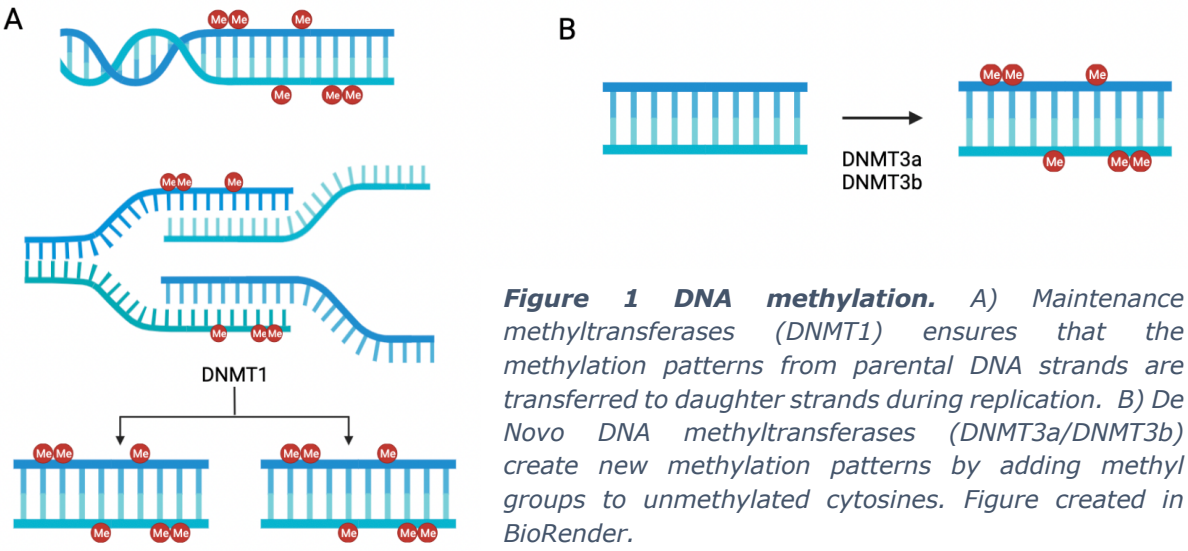

Figure 1 DNA methylation. *A) Maintenance methyltransferases (DNMT1) ensures that the methylation patterns from parental DNA strands are transferred to daughter strands during replication. B) De Novo DNA methyltransferases (DNMT3a/DNMT3b) create new methylation patterns by adding methyl groups to unmethylated cytosines. Figure created in BioRender.*

1.1.2 DNA demethylation

DNA demethylation, the removal of a methyl group from a cytosine, can either be passive or active. Passive DNA demethylation occurs in the absence of DNMTs during DNA replication, while active demethylation is a replication-independent process where the methyl group is directly removed from the strand via enzymes [10]. Oxidative DNA methylation is one of the active demethylation pathways (Figure 2), where ten-eleven translocases (TET), Thymine-DNA glycosylase (TDG), and base excision repair (BER) are involved [11]. First, TET-enzymes oxidate the methyl group and convert 5mC into the demethylation intermediate 5-hydroxymethylcytosine (5hmC) [11-13]. 5hmC recruits methyl CpG binding protein 2 (MeCP2), a "reader" that recruits the transcriptional activator cAMP-response-element-binding protein 1 (CREB1) [3]. MeCP2 also contributes to transcription by making the chromatin more attainable for transcription factors [14]. Thus, demethylation impacts transcription through hmC-modifications. Furthermore, TET generates 5-formylcytosine (5fC) and 5-carboxylcytosine (5CaC) on the previously methylated site [15]. Maintenance DNA methyltransferases (DNMT1), which are in charge of the cytosine methylation in DNA strands, do not recognize 5hmC, 5fC, or 5caC [16]. Hence, the nascent DNA strand will not be methylated at these specific oxidated sites during DNA replication. TDG takes part in the process, as it recognizes 5fC and 5caC. The enzyme excise thymine (T: G), 5fC, and 5caC, leaving the site abasic [16, 17].

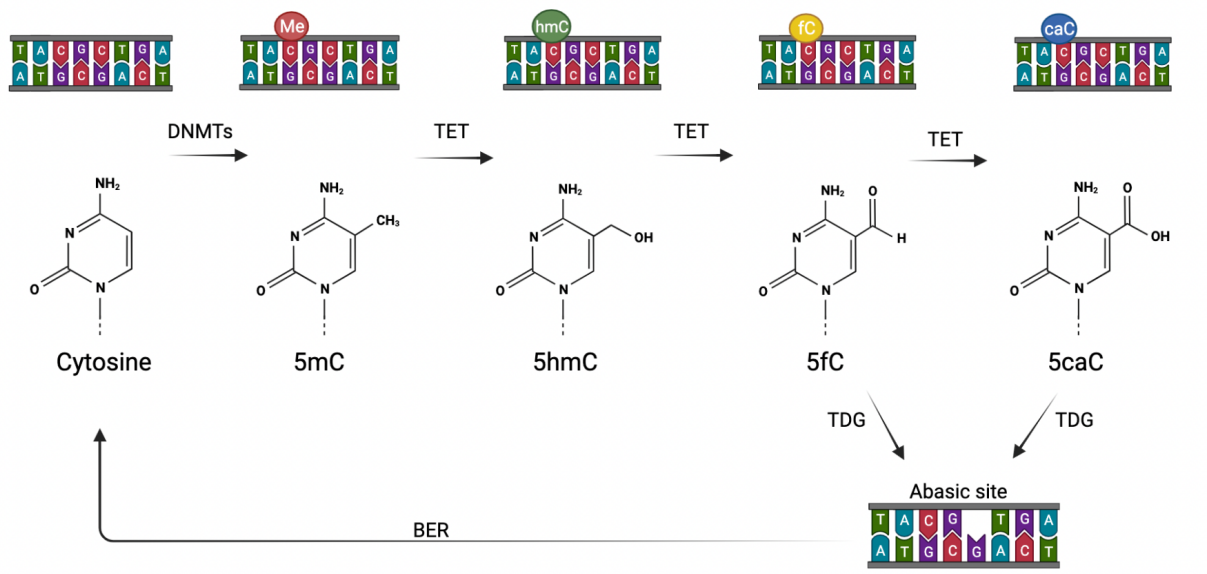

Figure 2 Active/TDG-mediated demethylation: *Cytosines that have been modified with methyl groups may be demethylated by TET-enzymes. TET-enzymes first oxidize 5mC to hmC, then to 5fC and/or 5CaC. TDG recognizes 5fC/5caC and excises the modified cytosine, leaving the site abasic. Through BER, a new unmodified cytosine is inserted. Figure created in BioRender.*

The cytosine will not be modified due to TDG, and the abasic sites are fixed through base excision repair (BER). BER is one of the main DNA repair mechanisms that occur when bases in DNA strands are damaged [18]. Faulty or damaged bases are efficiently removed by damage-specific DNA glycosylases (e.g., TDG) that cleave the N-glycosidic bond between the deoxyribose and the base, leaving the site abasic (AP) [18-20]. Furthermore, an AP-endonuclease (APE) recognizes the AP site and generates a 3´OH group. Then, a DNA polymerase uses the OH-group as a substrate, allowing it to insert the missing base [18, 20]. Finally, a DNA ligase seals the nick in the strand [18-20]. BER is an important mechanism considering disease prevention, due to its function of DNA repair [21]. This has been seen among others, with neurodegenerative diseases and aging, where elevated DNA damage and DNA repair deficiency has been observed [20].

1.1.3 TDG – Gene & Protein

The *Tdg*-gene encodes the G/T mismatch-specific thymine-DNA glycosylase (TDG) and is a part of the uracil-DNA glycosylase (UDG) superfamily [22]. One of the functions of the superfamily is DNA repair [15, 23]. TDG mediates the correction of G/T mismatches to G/C pairs through hydrolyzation of the carbon-nitrogen bond that keeps the sugar-phosphate group in the DNA and the mismatched thymine together [23]. As a result, the thymine is released. TDG can also release thymine from mismatched C/T and T/T, but the strongest affinity is towards G/T. One of the most pivotal roles of the gene is found in the TDG-mediated demethylation pathway [12, 15, 24]. In addition, TDG has also been observed interacting with DNMT3a, transcription factors, and histone acetyltransferases, suggesting an important association with gene regulation [22, 25-27].

1.2 The TDG mouse model and rAAV-Cre viral tools

It is not possible to create complete TDG-knockout mice, as knockout of TDG is embryonically lethal [22]. For a postnatal gene knockout, it is possible to use the Cre-loxP system with rAAV-Cre viral tools. Recombinant Adeno Associated Viruses (rAAV) can be genetically programmed with a promoter and gene product of choice. In this way, viral tools can be used to efficiently introduce tissue specific Cre expression into an organism. Cre is a 38-kDa DNA recombinase derived from the bacteriophage P1 [28, 29]. The specific DNA sequence called *loxP* (locus of x-over, P1) site is recognized by the recombinase, leading to a site-specific deletion of the DNA sequence between two *loxP* sites. Each *loxP* site is a 34 bp long sequence with an 8 bp core and two 13 bp inverted and palindromic repeats [28, 30, 31]. Recombination may be accomplished through different reactions, such as excision, inversion, translocation, and cassette exchange, as determined by *loxP* site orientation [30]. For gene excision the *loxP* sites are oriented in the same direction. The recombinase recognizes the repeated *loxP* sites and the flanked DNA sequence is excised into circular DNA with the silenced gene (Figure 3) [28, 31]. For a tissue specific recombination in hippocampal neurons, rAAV carrying a synapsin promoter controlling Cre-expression can be applied [32].

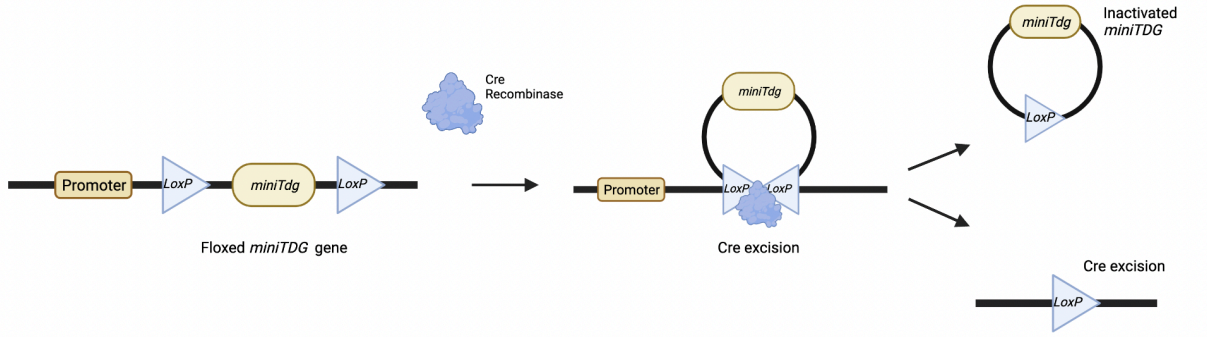

Figure 3 Cre-LoxP system. *The flanked DNA sequence with the target gene is being excised by a Cre-recombinase that recognizes two repeated loxP sites. The excision results in one knockout DNA and one circular DNA with an inactivated target gene. Figure created in BioRender.*

A reporter gene is inserted into the DNA sequence, downstream of a flanked stop codon, e.g., GFP (green fluorescent protein), in order to visualize Cre-expression. Cre-recombinase will excise the stop codon into circular DNA due to the two *loxP*-sites surrounding it [30]. When the stop codon is removed, gene transcription will continue and GFP is expressed and will release a fluorescent signal (Figure 4).

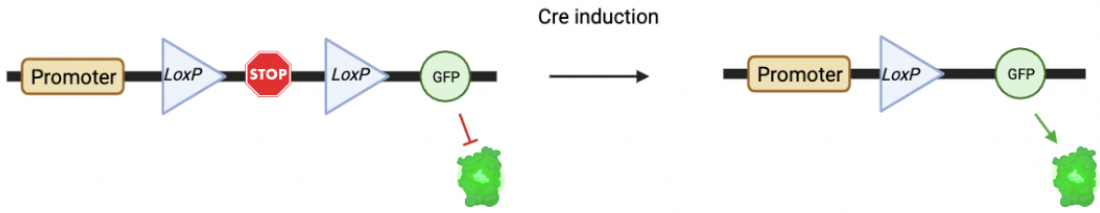

Figure 4 GFP reporter gene. *The Cre-recombinase recognizes the repeated LoxP-sites and excises the stop codon, resulting in GFP expression. Figure created in BioRender.*

1.3 The role of DNA-methylation in neural development, memory, and learning

For many decades, it was believed that modifications of neuronal circuits, neurogenesis, and de novo neuronal connections only happened during development. However, more recent studies have found a consensus that synaptic plasticity and ongoing adult neurogenesis are specifically apparent in the hippocampus, where synapses and neurons are continuously rearranged [33, 34]. Aging impacts dendritic and synaptic structures of mature hippocampal neurons in specific regions, but plasticity remains throughout life. Neurons of the hippocampus create a foundation of learning and memory, indicating that epigenetic modifications of these neurons may regulate memory consolidation too [2].

As there is a connection between learning and hippocampal plasticity, it is important to highlight the DNA-methylation part in this. Previously, it was suggested that DNA methylation patterns remained constant after embryonic development, but new research has found evidence that methylation patterns not only continue to change with age but also take an important role in memory consolidation and learning [4-6]. Studies have among others shown that synaptic plasticity in the adult hippocampus is regulated by DNMTs, through stable and dynamic changes of DNA methylation in learning relevant genes, such as *Reelin*, *Calcineurin*, and *Bdnf*, during cellular and systems consolidation [35, 36]. Furthermore, in a rat model where hippocampal DNMTs were inhibited, the rats were not able to consolidate memories after fear conditioning [37]. DNMT inhibition has also been found to prevent long-term potentiation (LTP), indicating a pivotal role for DNA methylation in memory formation [2]. Hippocampal neurons that go through LTP are believed to be the foundation of the neuroplasticity that is involved in memory formation and learning [2]. Furthermore, DNA methylation may repress gene expression of proteins that would normally inhibit the formation of long-term plasticity [36]. As DNA methylation has been shown to cause long-term changes in neuronal gene expression, the overall function state is affected by DNA methylation, making it critical for memory formation [38]. In addition, DNA-methylation in the brain declines as the individual ages, which coincides with a decline in learning and memory [39].

Hippocampal methylation patterns are not random, and findings show that the development of neuronal tubes and embryonic stem cells are developmentally regulated by a DNA methylation program (DMP) [40, 41]. Through epigenetic marks such as 5mC and 5hmC in the CA and DG, it has been observed that DMP both prenatally and postnatally regulates neuronal differentiation and maturation spatiotemporally in the hippocampus [41]. Furthermore, pyramidal cells of CA and granule cells of DG, modulate synaptic plasticity and memory consolidation, which are dynamically regulated through active demethylation [41]. During active demethylation, 5mC is converted into 5hmC, which takes part in neuronal maturation and is seen abundantly in the nervous system [42]. 5hmC is not only an intermediate but also a stable epigenetic mark involved with increased gene expression, especially genes relevant to synapses and development [41-43]. In general, hmC increases in various brain tissue throughout life, notably during neuronal differentiation [42, 44]. Accordingly, if the neuronal functions are epigenetically modified, it will impact learning and memory.

1.4 DNA methylation and demethylation in the aging brain

Cognitive impairments, loss of neural plasticity, and brain function deterioration are commonly seen with aging. The decline is often associated with epigenetic alterations, such as in DNA methylation [45, 46]. Consequently, global DNA hypomethylation and hypermethylation of CpG islands have been seen in various aged brain regions, such as the frontal and temporal cortex [47, 48]. That is why genome-wide DNA methylation changes may be used as biomarkers for cellular aging [49, 50]. DNA methylation has been observed to be associated with the chronological age of cells in different brain regions, such as glial cells and neurons [50]. Cognitive impairments are a consequence of the age-induced dysregulation of the DNA methylation machinery in the hippocampus, which has been observed in mice models where epigenetic markers in the hippocampus of young and aged mice have been compared [45]. Dnmt3a2 transcript levels have among others been seen to decrease in the aged hippocampus of mice when compared to young, which consequently would lead to hypomethylation. Furthermore, it has been suggested that cognitive abilities in young and aged mice are greatly impacted by hippocampal Dnm3a2 levels [51]. Another epigenetic age regulator that recently has been noticed is the ten-eleven translocase, TET2. TET-enzymes oversee the conversion of 5mC into 5hmC in TET-mediated active demethylation and TET2 has been observed to decrease, along with 5hmC, in the aged hippocampus of mice in association with regenerative decline [52]. These findings have been strengthened by data showing TET2 reduction cause impaired cognition and neurogenesis in the young hippocampus [52]. However, other findings show increased hippocampal 5hmC distribution in the DG and CA regions in aged mice compared to young mice, without changes in TET1-TET3 mRNA levels [53, 54]. More studies need to be conducted to find clear answers, but nevertheless, it is essential to keep up the maintenance of neuronal DNA methylation patterns in the brain, due to synaptic plasticity and memory formation, and their underlying dynamic gene expression changes [55-57].

Alterations in patterns of neuronal DNA methylation have not only been seen in aging but also in age-related neuropathies, such as Alzheimer's disease (AD) [45, 58]. The greatest risk factor for developing AD is age, and the aberrant age-related methylation patterns have been seen accelerated in AD [58]. Findings show both aberrant 5mC- and 5hmC-levels in the brain regions of AD patients compared to non-demented patients, such as decreased 5mC levels in hippocampal CA1 and decreased 5hmC levels in CA3 and DG [47, 59]. The aberrant DNA modifications cause epigenetic dysregulation of gene transcription, e.g., decreased 5mC levels in the entorhinal cortex layer II in AD patients affect DNMT1 and MeCP2 levels [60]. In AD pathology, aberrant 5mC- and 5hmC levels correlate with AD hallmarks, such as amyloid-β plaque and neurofibrillary tangle (NFT) formation [61]. With increased knowledge of the molecular basis of this neuropathy, new possible targets for AD therapy are created. However, age in general causes brain function impairment through dysregulation of epigenetic genes, and more investigation is needed to fully understand the age-dependent deterioration of the brain.

1.5 Hippocampus

1.5.1 Hippocampal formation and anatomy

The hippocampal formation is an intricate neurological system in the temporal lobe that contributes immensely to cognition and memory consolidation due to an ongoing structural plasticity [33, 62]. It consists of brain regions such as the dentate gyrus (DG), subiculum, presubiculum, parasubiculum, entorhinal cortex (EC), and hippocampus proper [63]. The hippocampus proper includes the subfields of cornu ammonis (CA), which are divided into CA1, CA2, and CA3. DG is made up of two excitatory cell types, granule cells and mossy fibers. The majority of the DG cells are granule cells located in densely packed granule layer, while the second type, mossy cells, are found subjacent to the hilus [64]. It is believed that cortical input patterns from EC are scattered throughout the granular cell layer of DG, making it possible for a sparse amount of firing granule cells to transmit a small significant portion of the total input [65]. The sparse amount of firing from the granule cells is connected to the principal cells of CA3, the pyramidal cells, through mossy fibers that function as axons. Together, the pyramidal and granule cells create the hippocampal formation through an intrinsic circuitry [2].

1.5.2 Hippocampal function

The hippocampus is a part of the limbic system, a system that is important in association with emotional response, behavior, and survival. In the hippocampus, the limbic system works among others, through learning and memory formation [2]. Memory formation is thought to be a result of the neuroplasticity caused by hippocampal neurons that undergo long-term potentiation (LTP) [66]. LTP is a synaptic transmission that is long-lasting, begins rapidly, works in hand with brain rhythms, and other qualities that are needed for memory storage [67]. These hippocampal neurons make it possible to encode information about sensory, spatial, or temporal changes in daily experiences, and it has even been suggested that the hippocampal neurons may sort each experience into specific units [2, 68].

Information that is associated with memory is organized in both spatial and non-spatial pathways. Spatial information is needed to understand the environment and is interpreted through hippocampal neurons called place cells. It has been observed that place cells fire at a high rate in the place field, which is a specific location in the environment [69]. The spatial pathway also receives cortical input from the medial entorhinal cortex (MEC) in the form of grid cells, boundary cells, and head direction cells, from the post-rhinal cortex [70, 71]. It has been observed in animal models that when the animal explores a new environment, the grid cells fire in multiple locations, that some of the grid cells are modulated by the animal's head direction, and that when the animal reaches the edge of a new environment, e.g., a wall, boundary cells will fire to provide information to align with the grid cells [70, 72-74]. A similar firing pattern has also been observed in other hippocampal regions such as the subiculum, presubiculum, and parasubiculum, which are anatomically connected to the MEC [70]. On the other hand, in the non-spatial pathway, the lateral entorhinal cortex (LEC) receives cortical input from the perirhinal cortex [70, 71]. It has been observed that neurons in LEC react to different items, e.g., odors and

pictures of objects, but when movement-related events occur, no strong spatial firing is detected [70].

Memory consolidation and storage are also seen in other hippocampal regions. Pyramidal cells from CA3 project to pyramidal cells in CA1 through axons known as Shaffer collateral. Excitatory input is conveyed to CA3 in three ways: through recurrent Shaffer collateral, through the mossy fiber from granule cells in DG, and through the perforant path [75, 76]. Due to recurrent collateral and observations of modified synaptic strength that may store memories, it has been suggested that CA3 might be a memory network [75].

1.6 Medial entorhinal cortex (MEC)

1.6.1 Entorhinal cortex in rodents

In primates, the entorhinal cortex (EC) is a significant hippocampal region found in the medial temporal lobe (MTL), while in rodents it is divided into lateral and medial subregions [77]. The different subregions have different functions in association with their cell types. MEC, with its grid cells and head-direction cells, receives input from the parahippocampal cortex about spatial information, and neurons in the LEC fire to individual objects in the environment, due to input from the perirhinal cortex [77, 78]. It is difficult to localize the rodent homolog of MEC/LEC in humans. However, it has been suggested that the regions may not be anatomical locations, but cytoarchitectonically areas, as similar functions have been seen according to their cell types [79]. Also, when it comes to neuropathies, e.g., AD, it has been seen a similar pathological pattern, where the disease has affected both lateral and medial EC strips in humans and in both MEC and LEC in rodents [80].

1.6.2 MEC circuitry

The MEC is divided into four principal cell layers, creating a far-reaching network to process spatial information [81]. MEC neurons show grid field activity in a hexagonal firing pattern, but the mechanism behind remains unclear [82]. Furthermore, layer II consists of stellate cells and pyramidal cells that create a local circuit within the region [82, 83]. Stellate cells have superficially branching dendrites and large sag potentials [83]. They also express reelin, an extracellular glycoprotein that contributes to memory and cognition, as altered reelin expression may influence synapses and firing patterns [83-85]. Terminals from the stellate cells are the major source of excitatory input from MEC to hippocampal CA3 and DG [83]. On the other hand, pyramidal cells are found in tight clusters that receive cholinergic input [86, 87]. In the CNS, cholinergic innervation is crucial in the regulation of learning and memory consolidation, and alterations have been observed in aging and AD [87, 88]. Pyramidal cells also express WFS-1 and calbindin, a calcium- and buffering protein that is involved in synaptic plasticity [85, 87, 89]. Through different connections, the principal cells create microcircuits, where the stellate cells are linked through parvalbumin neurons that are fast-spiking and somatostatin-positive neurons that spike slower [83, 85]. Furthermore, the pyramidal cells are linked to the microcircuits through 5-HT 3a positive interneurons [85].

1.7 Aim

The project's main aim is to investigate the accumulation of DNA demethylation intermediates during aging. I will assess the levels of 5hmC, 5fC, and 5CaC in the MEC and hippocampal CA1 in young (3 months old) and aged (18 months old) wildtype mice.

The second aim of this study is to establish a reliable method for the conditional manipulation of TDG expression in neurons using the Cre-loxP system. This is of interest, as the DNA demethylation intermediates (5fC and 5CaC) are excised by TDG in TDG-mediated DNA demethylation. For this purpose, TDG-depletion will be assessed in the hippocampal region of *LoxP-MiniTdg*$^{+/+}$ mice (3 to 6 months) after rAAV-Cre injection, with focus on infection efficiency, immune response, and molecular TDG levels after depletion.

2. Material and Methods

2.1 Mouse model

The mice for the age-dependent regulation experiment were wildtype (WT, background C57/BL6N) and immunohistochemistry analysis was performed on samples from 3- and 18-months old animals. The mouse model used for the TDG depletion experiment was *LoxP-MiniTdg*$^{+/+}$ (background C57/BL6J) mice (3 to 6 months). TDG was depleted with viral infections in the hippocampus using rAAV-Cre viral tools. Both mouse models were bred in the animal facility of the Laboratory Centre of St. Olavs Hospital in Trondheim, Norway. The mice had food and water access *ad libitum*, the light-dark cycle was 12:12, and the room temperature was 25^{o}C.

2.2 Brain perfusion

The pre-weighted animal was first anesthetized by isoflurane (1 mL) gas in an airtight box. When the animal was anesthetized by the gas, the animal would be further anesthetized by an intraperitoneal injection of pentobarbital (2 mg/g), which eventually put the animal down due to overdose. Hence, the procedure had to be done quickly. To confirm that the animal was fully anesthetized, pain reflexes were tested before starting the procedure. First, an incision was made into the animal´s sternum, removing its ribcage, and exposing its heart. The left lung was then mobilized, to expose descending aorta. The descending aorta was clamped to ensure thorough brain perfusion. Furthermore, the right atrium was nicked, followed by a constant saline injection (60 mL) in the left ventricle to perfuse the brain. After saline perfusion, the brain was collected by removing the occipital bones by the atlas and axis vertebrae, followed by gentle removal of the left and right parietal bones, and the frontal bones. The right hemisphere was collected for frozen sectioning and stored in 4% paraformaldehyde (PFA), while the left hemisphere was microdissected into DG, CA1, and CA3 for RNA extraction and RT-qPCR, and immediately stored in -80 ^{o}C. In addition, about 1 cm of the animal's tail was collected for genotyping.

2.3 Genotyping

Ear clippings or tail samples were lysed in lysis buffer (10 mM Tris, 1M KCl, 0,4% NP-40/Igepal CA630 Sigma, 0,1% Tween20) with Protein kinase K (10 mg/mL) overnight, incubating in 59 ^{0}C. The following day, the samples were heated to 95 ^{0}C for 30 minutes, followed by centrifugation (14.000 rpm, 20 minutes) before DNA was collected from the supernatant. DNA was diluted (1:10) and added to a PCR mix with a total volume of 10 µL containing Taq Master Mix (10XPCR Buffer, 2,5/10 mM dNTPs, 5U/mL paq5000, 50 mM $MgCl_2$), ddH_2O, and 0,5 µM of each forward and reverse primer (Table 1).

Table 1 Primers used for genotyping

Oligo name	Sequence	Application
Compl. mTDGi F	AAATACTCTGAGTCCAAACCGGG	Genotyping *miniTdg*
TDG C R	TGGTGAATCCGATGCCGTACTTG	Genotyping *miniTdg*
CAG GFP F	CTTCAGCCGCTSCCCCGACCACA	Genotyping *gfp*
CAG GFP R	ATCGCGCTTCTCGTTGGGGTCTTT	Genotyping *gfp*

The PCR program was set to 95 ^{0}C for 3 minutes, followed by 42 cycles of 95 ^{0}C for 30 seconds, 64 ^{0}C for 30 seconds, and 72 ^{0}C for 1 minute. Afterward, the program was set to 72 ^{0}C for 5 minutes, before ending at 4 ^{0}C infinite. For gel electrophoresis, a 2% Agarose gel was applied, made of Standard Agarose (LE Agarose, BioNordica, Cat. #BN50004), TAE buffer (Tris Base, Glacial Acetic Acid, 0,5M EDTA), and 1% SybrSafe (ThermoFisher/Invitrogen, Cat. #S33102). 5 µL of 100 bp DNA ladder (New England Biolabs) and PCR samples containing 1% 6X DNA loading dye (New England Biolabs, Cat. #B7024A) were aliquoted into the wells, and the gel ran at 120V for 40 minutes. The results were visualized on the imaging system, ChemiDoc™ MP, from Bio-Rad.

2.4 RT-qPCR

To investigate the presence of hippocampal TDG levels after viral infections, a pilot experiment of RT-qPCR was performed. First, RNA was extracted from hippocampal CA1, CA3, and DG from the left hemisphere. For the RNA extraction, tissue samples were placed in tubes with 3-5 zirconium beads and 300 µL RLT buffer (RLT Lysis Buffer, QIAGEN, Cat. #1015762) and homogenized on a MagnaLyzer (Rosche) for 10 seconds and at the speed of 5000. Furthermore, RLT buffer was added in 0.75 volume ratio to the original sample, homogenized, and centrifuged at full speed for 3 minutes. Ethanol was added to the homogenized sample (1:1) before the whole volume was transferred to a RNeasy spin column placed in a 2 mL collection tube. Using RW1- (RW1 Wash Buffer, QIAGEN, Cat. #1015763) and RPE buffer (20% RPE Wash Buffer in 70% Rnase-free Ethanol, QIAGEN, Cat. #1017974), the column was washed in accordance with the RNA extraction guide from QIAGEN (Rneasy ® Mini Handbook, QIAGEN, 2019), and extracted RNA was collected with Rnase-free H_2O (Rnase Free Water, QIAGEN, Cat. #1017979). After the RNA extraction, a Dnase treatment was performed with TURBO™ DNAase kit (2U/µL) (ThermoFisher, Cat. # AM2238), to minimize genomic DNA carryover. 10X TurboDNase buffer (ThermoFisher) was added to the RNA sample with a volume of 0.1 of the original sample, followed by 1 µL TurboDNase (ThermoFisher), and incubation for 20 minutes at 37 ^{o}C. Furthermore, Dnase inactivation reagent (ThermoFisher) was added in the same 0.1 volume ratio to the RNA samples, followed by incubation for 5 minutes at room temperature. The RNA samples were centrifuged at 10,000 rpm for 90 seconds before the supernatant was collected, and RNA was quantified using the NanoDrop spectrophotometer (ND-1000, NanoDrop). The final step before RT-qPCR was cDNA synthesis, where High-Capacity cDNA Reverse Transcription kit (ThermoFisher, Cat. #4368814) was applied. Master Mix, containing 2 µL buffer, 0,8 µL dNTPs, 1 µL MMLV, 2 µL Random Primers, nuclease-free H_2O (Millipore), and RNA, was added into PCR tubes. In this protocol, the total volume of nuclease-free H_2O and RNA was 14,2 µL. Using the results from the NanoDrop, The RNA concentration was calculated to get the wanted RNA volume (>100 ng). To reach the wanted total volume,

nuclease-free H_2O was added as compensation. The cDNA synthesis occurred on a thermocycler with a program set to 25°C for 10 minutes, 37°C for 2 hours, 85°C for 5 minutes, and 4°C infinite. For the RT-qPCR, a 1 ng/µL RNA dilution was applied, along with one Master Mix per primer, containing Power SYBRgreen (Applied Biosystems, Cat. #100029284), forward primer, reverse primer, and nuclease-free H_2O (Millipore). The applied primers, miniTDG (Sigma-Aldrich), TDG exon (Sigma-Aldrich), and GAPDH (Sigma-Aldrich), can be seen in Table 2. RNA samples and Master Mix were aliquoted into 96-wells in a 3:10 ratio and analyzed on StepOnePlus, RT-qPCR system (Applied Biosystems, Thermo Fisher Scientific), with corresponding software.

Table 2 Primers used for RT-qPCR.

Oligo name	Sequence (5´ - 3´)
miniTDG/TDG UTR F	AGGGCTGCAGTTCTAATCG
miniTDG/TDG UTR R	TTGACTCTACCATATAACTGCTCC
Tdg exon 6/7_F	GCCACGAATAGCGGTGTTTAATG
Tdg exon 6/7_R	GGCATGACGTAGCACAGAGT
mGAPDH_qPCR_F	AGGTCGGTGTGAACGGATTTG
mGAPDH_qPCR_R	TGTAGACCATGTAGTTGAGGTCA

2.5 Frozen sectioning

For frozen sectioning, CryoStar NX40 from Thermo Scientific was applied. The temperature of the chamber and objective was −20 ^{0}C. Before sectioning, the brain tissue was fixated in 4% PFA for at least 48 hours. The right hemisphere was used for sectioning and mounted on the corresponding metal socket with OCT mounting medium. For rapid and complete freezing of the brain, freezing aerosol spray (PRF 101/520 ML GREEN NFL) was sprayed over the mounted tissue, and cryogenic settings on the instrument were utilized. Brain tissue was sectioned into 30 µm thin samples and stored in PBS x1 containing 0,03% ProClin™ 300 (Sigma-Aldrich, Cat. #48912-U) at 4 ^{0}C.

2.6 Immunohistochemistry

Immunohistochemistry was performed to analyze demethylation intermediates in MEC and Cre-induced GFP expression after TDG depletion in hippocampal DG, CA1, and CA3. The tissue applied for staining was 30 µm thin medial and lateral sections from the right hemisphere. For antigen retrieval, brain sections were incubated in preheated 40 mM trisodium citrate (Trisodium citrate 5,5 hydrate, Merk-Millipore 1.06431.1000) solution (pH 6 or pH10, depending on the distinct antibodies) for 3 minutes at 99 ^{0}C and cooled down to room temperature. After washing three times in 1xPBS (5 minutes/washing), the sections were incubated in blocking buffer (5% NGS/5% BSA/0,1% Triton X-100 in PBS) for two hours on a shaker at room temperature. This step was used to block unspecific bindings. Primary antibodies were diluted in dilution buffer (1% NGS/1% BSA/0,1% Triton in PBS), and sections were incubated with the diluted primary antibodies overnight at 4 ^{0}C

on a shaker. Antibody dilutions are presented in Table 3. Before adding secondary antibodies, the sections were washed three times (10 minutes, 20 minutes, and 30 minutes) on a shaker in 1xPBS-T (1xPBS and 0,1% Tween20) at room temperature. Then, the sections were incubated with the diluted secondary antibodies for 2 hours at room temperature on the shaker, protected from light. After being washed three times in 1xPBS-T, brain sections were mounted on coated slides and stained with DAPI-solution (1:5000 DAPI in 1xPBS for 1 minute). After a sequential wash with PBS and ddH_2O, the sections were cover-slipped with ProLong™ Gold antifade reagent with DAPI (Invitrogen, Cat. #P36935) and dried at room temperature and protected from light.

2.6.1 Antibodies

Primary antibodies used for immunohistochemistry in this study are presented in Table 3. In general, antigen retrieval in 40 mM trisodium citrate with pH6 was sufficient. However, 40 mM trisodium citrate with pH 10 was necessary for proper antibody binding, with epigenetic markers and intermediates from TDG-mediated demethylation. Secondary antibodies are presented in Table 4.

Table 3 Primary antibodies.

Primary antibody	Isotype	Dilution	Manufacturer	Function
NeuN	mIgG1	1:500	Millipore, *Cat. #:* MAB377	Neuron nucleic marker. Staining of mature neurons.
GFP	mIgG2a rIgG	1:1000 1:1000	Thermo Fisher, *Cat. #:* A-11120 Invitrogen *Cat. #: A-11122*	Gene reporter. Applied for visualization of Cre-induced TDG depletion.
hmC	rIgG	1:1000	Activemotif, *Cat. #:39769*	Epigenetic marker for DNA demethylation intermediate.
caC	rIgG	1:1000	Activemotif, *Cat. #:61229*	Epigenetic marker for DNA demethylation intermediate.
fC	rIgG	1:1000	Activemotif, *Cat. #:61227*	Epigenetic marker for DNA demethylation intermediate.
Iba1	rIgG	1:2000	Wako, *Cat. #: 019-19741*	Microglia. Immune response marker.
GFAP	mIgG1	1:500	Cell signaling, *Cat. #:3670S*	Astrocyte. Immune response marker.

Table 4 Secondary antibodies.

Secondary antibody	Isotype	Dilution	Manufacturer
A488	mIgG2a	1:1000	Invitrogen, *Cat. #: A-21131*
	mIgG1		*Cat. #:* A-21121
	rIgG		*Cat. #:* A-11008
A555	rIgG	1:1000	Invitrogen, *Cat. #: A-21431*
A647	mIgG2a	1:1000	Invitrogen, *Cat. #: A-21241*

2.7 Fluorescence imaging

The immunohistochemically stained brain sections (30 µm) were imaged with confocal laser scanning microscope Zeiss® LSM 880, and the high-performance slide scanner Zeiss® Axioscan Z1, along with corresponding software, *Zen*. For the confocal analysis of DNA demethylation intermediates in MEC, a Plan-Apochromat 40X/NA oil immersion objective was applied. The experiments had the same channel settings for pinhole, gain, and intensity, in correlation with the absorbance from applied antibodies (anti-NeuN, anti-hmC, anti-fC, anti-CaC), for comparative purposes. However, the Z-stack height was adjusted according to each sample, using the channel for the neuronal marker NeuN, to define where the section depth started and ended. To get a better picture of the target region, a 5x8 tile scan overview was imaged, showing the whole MEC. The overview showed the different cell layers and three 1x1 tiles could be imaged. Hippocampal GFP-expression (Cre-induced TDG-depletion) and hippocampal immune response were analyzed with the confocal microscope in a similar manner, but with a different tile scan overview (2x4), regions (CA1/CA3), and antibodies (anti-NeuN, anti-GFP, anti-GFAP, anti- Iba1). CA1 was imaged with tile scan 1x3 and CA3 was 2x1. Visualization of GFP expression in hippocampus was mainly performed through Axioscan imaging, a method involving multispectral fluorescence scanning with a 20x/0.8 M27 Plan Apochromat objective. The signal from Dapi (A405 blue) staining was used to set the right focus with a LED-Module 365nm light source. After adjusting the light source intensity to set the coarse and fine focus, scan settings were adjusted to 20,9% light source intensity with 20 ms exposure time. The channel for GFP (A488 green) applied a LED-Module 470nm light source, where light source intensity was set to 40,0% and the exposure time was set to 30 ms, while the channel for NeuN (A647 magenta) applied a LED-Module 625nm light source set to 30,0% intensity and 75 ms exposure time. In the end, the images were edited in the software ImageJ (Fiji).

2.7 Image analysis

TDG-meditated demethylation intermediates were visualized and quantified by using the 3D-imaging software IMARIS Surfaces (Version, 9.3.0, Oxford Instruments). The quantification method was based on the current brain region. First, a threshold was defined by two times the mean intensity volume from the target channel. Then, the signals from the image were made into voxels on a surface (1), which presented the signal amount as the *number of voxels* (Figure 5A). The number of voxels was divided by the *total volume*

of the target region, MEC-layer II/III or CA1 pyramidal layer, and multiplied by 100 µm^3, in order to determine voxels per region volume. For CA1, only the pyramidal layer was masked and used for defining the number of voxels, because including the whole surface would give a misleading value (Figure 5B*)*. The result defined the ratio of voxels/intermediates found in the target region, and was calculated through the presented formula:

$$Voxel\ ratio = \frac{Number\ of\ Voxels}{Total\ Volume} * 100\ \mu m^3$$

Due to less detected demethylation intermediates in MEC of young mice, unspecific binding in the form of lines was created. This was corrected by creating a new surface (2) where the threshold was set to 3.5 times the mean intensity value, which eliminated the unspecific lines. The number of voxels from surface 2 was subtracted from the number of voxels from surface 1, and the number of voxels sum was used in the formula applied for ratio calculation.

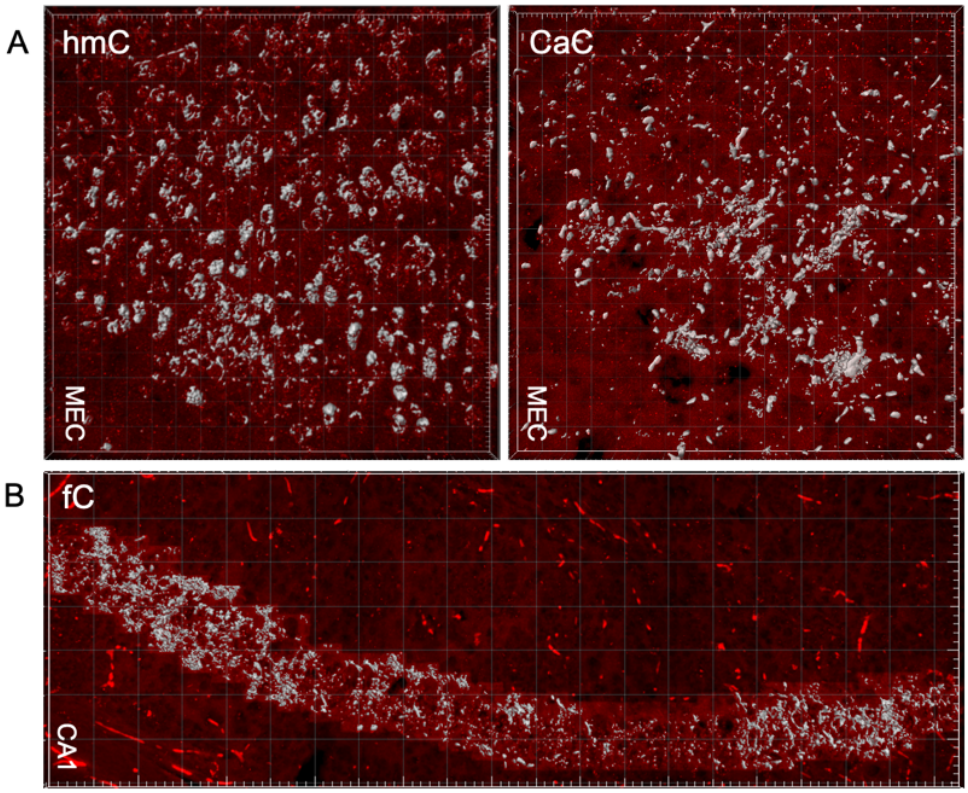

Figure 5 Image analysis in IMARIS 9.3.0. *A) Images presenting 5hmC- and 5CaC-staining in MEC, where the whole cell layer volume is included in calculating the voxel ratio of demethylation intermediates. The white marks visualize the number of voxels/intermediates on the surface. B) Image presenting 5fC-staining in hippocampal CA1, where only the voxels/intermediates that are visualized in the pyramidal cell layer are accounted for in the calculations.*

2.8 Statistical analysis

The software Prism 9 from GraphPad Software (Version 9.3.1) was applied for the statistical analysis, considering differences in immunoreactive signal in MEC and CA1 between 3- and 18-month-old mice (n>4 in both age groups). First, a mathematical model was applied to identify possible outliers. Then, a normality test was done to determine if there was a normal distribution, followed by an unpaired t-test (two-tailed), as two different age groups were going to be compared. The unpaired t-test was applied to examine whether the difference between the DNA demethylation intermediate levels in MEC and CA1 in young and old mice was statistically significant or not. For MEC, the statistical values came from the voxel ratio average from three different cell layers in 3- and 18-month-old mice (total n=10) from each target signal (5hmC, 5fC, 5CaC). While for CA1, the values came from the pyramidal layer from each sample of young and aged mice.

3. Results

3.1 Accumulation of DNA demethylation intermediates during aging

Global genomic DNA hypomethylation has been observed in aging, and it is involved in genome instability in aging and in age-related pathologies [90, 91]. However, age-associated DNA hypermethylation events have also been observed in promoter sites correlating with gene suppression, but in a lower degree [91, 92]. Many genome-wide studies of age-dependent alterations of methylation patterns have been performed on peripheral blood cells, but alterations have also been observed in other tissues, such as the cerebral cortex, cerebellum, and hippocampus [53, 93-95]. Here, I compared the DNA demethylation intermediate levels in MEC and in CA1 of the hippocampus (HPC) in 3- to 18-month-old mice. I investigated the levels of oxidative DNA demethylation intermediates through immunohistochemical staining of epigenetic markers (5hmC, 5fC, 5caC) in wildtype (WT) mice, to get a better understanding of age-dependent DNA demethylation and how it is regulated. The fluorescent signal detected from the epigenetic markers was analyzed in the 3D-imaging software IMARIS, using a method that quantifies the number of fluorescent voxels per region volume (e.g., 100 µm3) in the MEC-layer II/III and in the CA1 pyramidal layer.

3.1.1 Regulation of 5hmC in mouse MEC and HPC during aging

5hmC signal was detected in MEC in 3- and 18-month-old (n=5 for each age group) mice. A slightly higher level of 5hmC was detected in the aged MEC-layer II/III compared to young mice (Figure 6A-B), but the difference was not statistically significant (Figure 6C, p=0.2058, unpaired t-test). Similar levels of 5hmC were also detected in the CA1 pyramidal cell layer of young and aged mice (Figure 6D-F, young (n=4); aged mice (n=5), p=0.5720, unpaired t-test). The result suggests that there are no significant differences in 5hmC-levels in MEC and CA1 between young and aged mice.

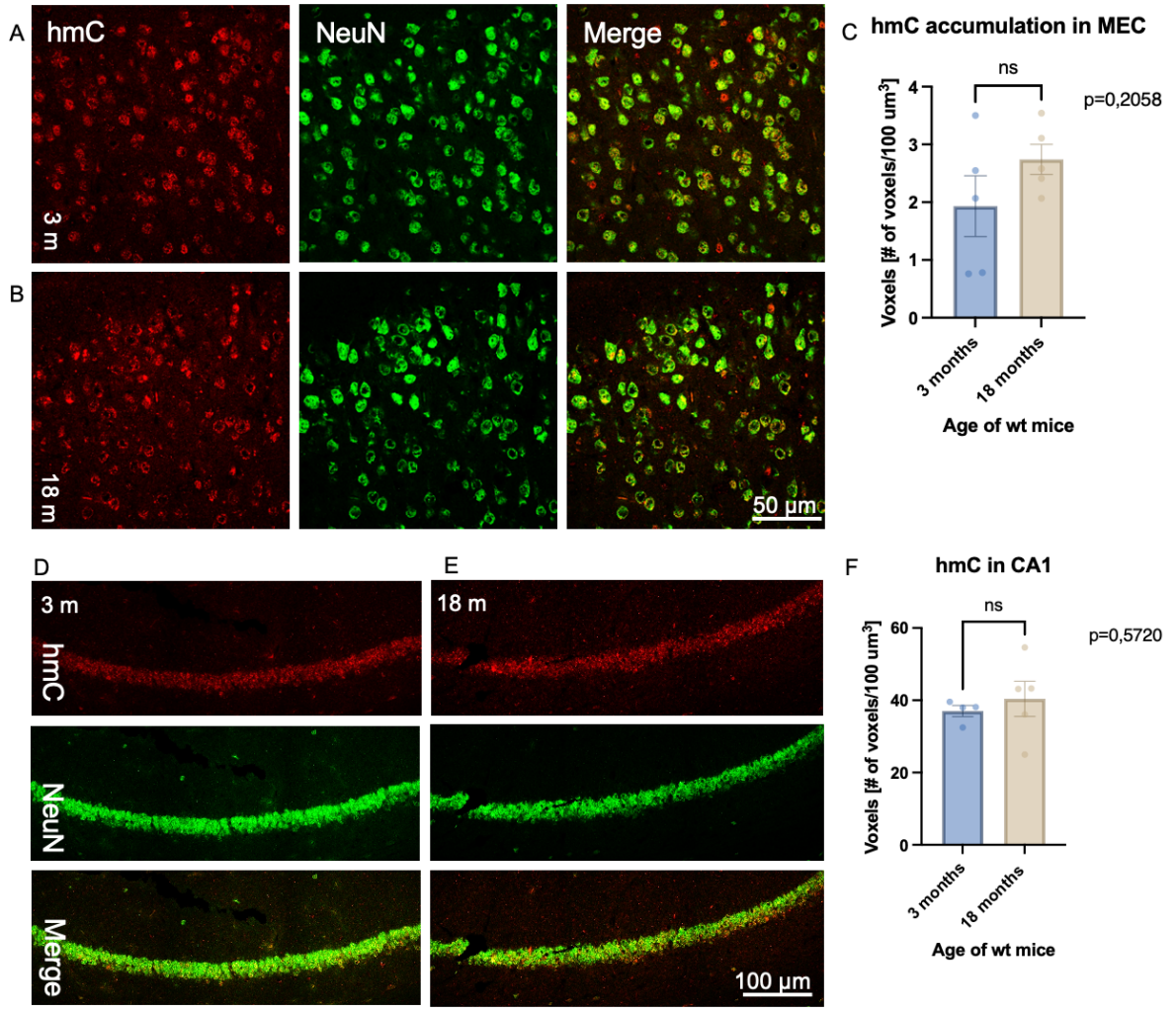

Figure 6 5hmC levels in young and aged MEC and CA1 A/B) Immunofluorescent staining of 5hmC in the MEC. *5hmC signal (red) is detected in MEC in both young (3 m) and aged (18 m) mice. NeuN-staining (green) presents neurons in the MEC layers II and III. Scalebar 50 µm.* ***C) The histogram shows the level of 5hmC in young and aged MEC (total n=10).*** *No significant differences in 5hmC levels were detected comparing young and aged mice in MEC (No statistical significance; unpaired t-test, p-value >0.05)* ***D/E) Immunofluorescent staining of 5hmC in the hippocampal CA1.*** *5hmC signal (red) is detected in the pyramidal cell layer of CA1 in both young (3 m) and aged (18 m mice). NeuN-staining (green) presents neurons of the pyramidal cell layer of CA1. Scalebar 100 µm.* ***F) The histogram shows the levels of 5hmC in CA1 pyramidal neurons in the two age groups (total n=9).*** *No significant differences in 5hmC levels were detected comparing young and aged mice in CA1 (No statistical significance; unpaired t-test, p-value >0.05)*

3.1.2 Regulation of 5fC in mouse MEC and HPC during aging

5fC signal was detected in MEC in 3- and 18-month-old mice (n=4 and n=5 for the age groups, respectively). A clearly higher level of 5fC was detected in the aged MEC-layer II/III compared to young mice (Figure 7A-B), and the difference was statistically significant (Figure 7C, p=0.257, unpaired t-test). 5fC signal was also detected in the CA1 pyramidal cell layer in young and aged mice (n=4 for each group) (Figure 7D-E), where the highest levels were found in the aged mice. The difference was statistically significant (Figure 7F, p=0.066, unpaired t-test). The result suggests that the 5fC levels are significantly increased in aged MEC and CA1.

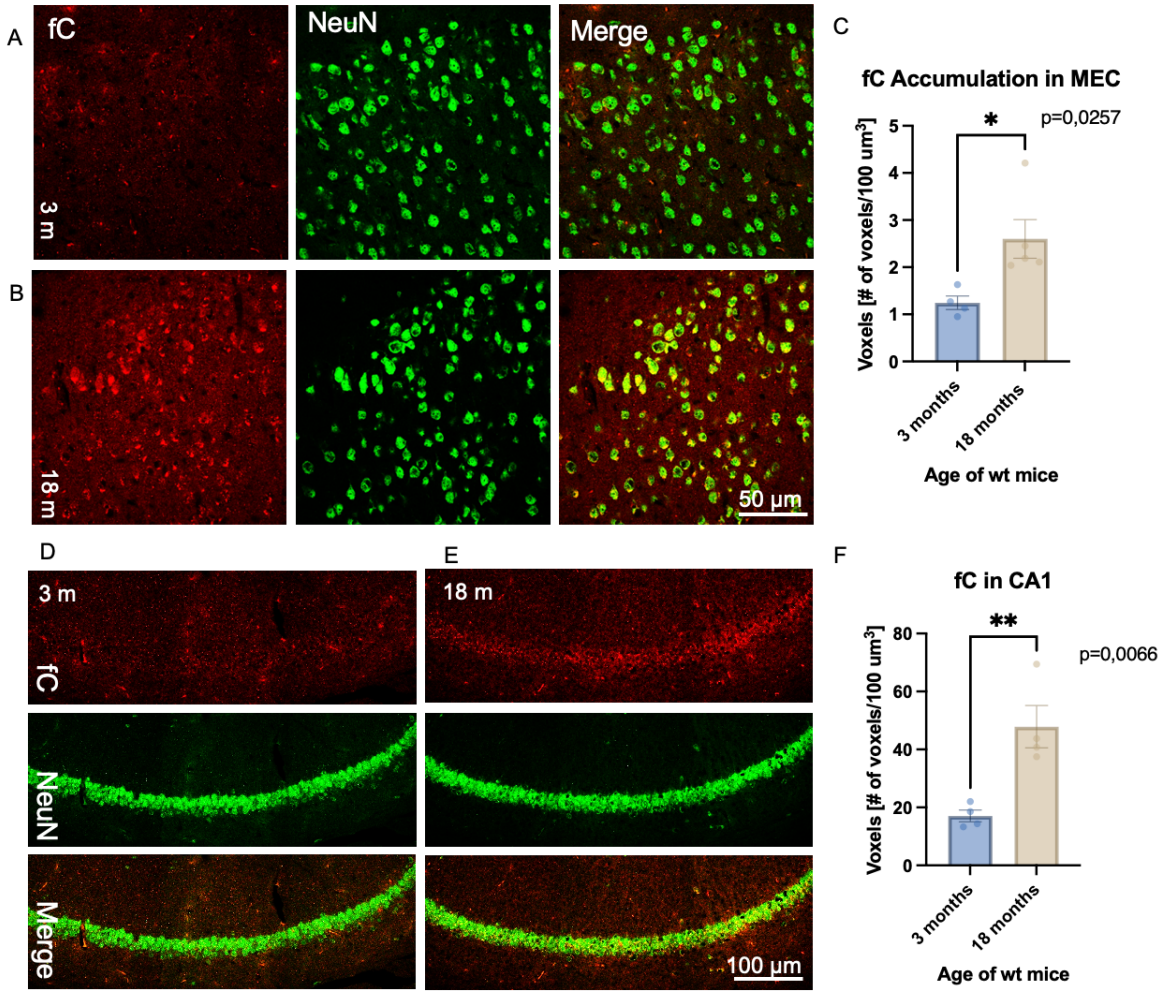

Figure 7 5fC levels in young and aged MEC and CA1 A/B) Immunofluorescent staining of 5fC in the MEC. *5fC signal (red) is detected in MEC in young (3 m) mice but the signal is stronger in aged (18 m) mice. NeuN-staining (green) presents neurons in the MEC layers II and III. Scalebar 50 µm.* ***C) The histogram shows the level of 5fC in young and aged MEC (total n=9).*** *A significant difference in 5fC levels was detected comparing young and aged MEC (Statistically significant; unpaired t-test, p-value <0.05).* ***D/E) Immunofluorescent staining of 5fC in the hippocampal CA1.*** *5fC signal (red) is detected in the pyramidal layer of CA1 in young (3 m) mice but the signal is stronger in aged (18 m) mice. NeuN-staining (green) presents neurons of the pyramidal cell layer in CA1. Scalebar 100 µm* ***F) The histogram shows the level of 5fC in CA1 pyramidal neurons in the two age groups (total n=8).*** *A statistical difference was detected comparing young and aged mice in CA1 (Statistically significant; unpaired t-test, p-value <0.05).*

3.1.3 Regulation of 5CaC in mouse MEC and HPC during aging

5CaC signal was detected in MEC in 3- and 18-month-old mice (n=4 and n=5 for the age groups, respectively). A clearly higher level of 5CaC was detected in the aged MEC-layer II/III compared to young mice (Figure 8A-B), and the difference was statistically significant (Figure 8C, p=0.0037, unpaired t-test). 5CaC signal was also detected in the CA1 pyramidal cell layer in young and aged mice (n=5 for each group) (Figure 8D-E), where the highest levels were found in the aged mice. The difference was statistically significant (Figure 8F, p=0.0001, unpaired t-test). The result suggests that the 5CaC levels are significantly increased in aged MEC and CA1.

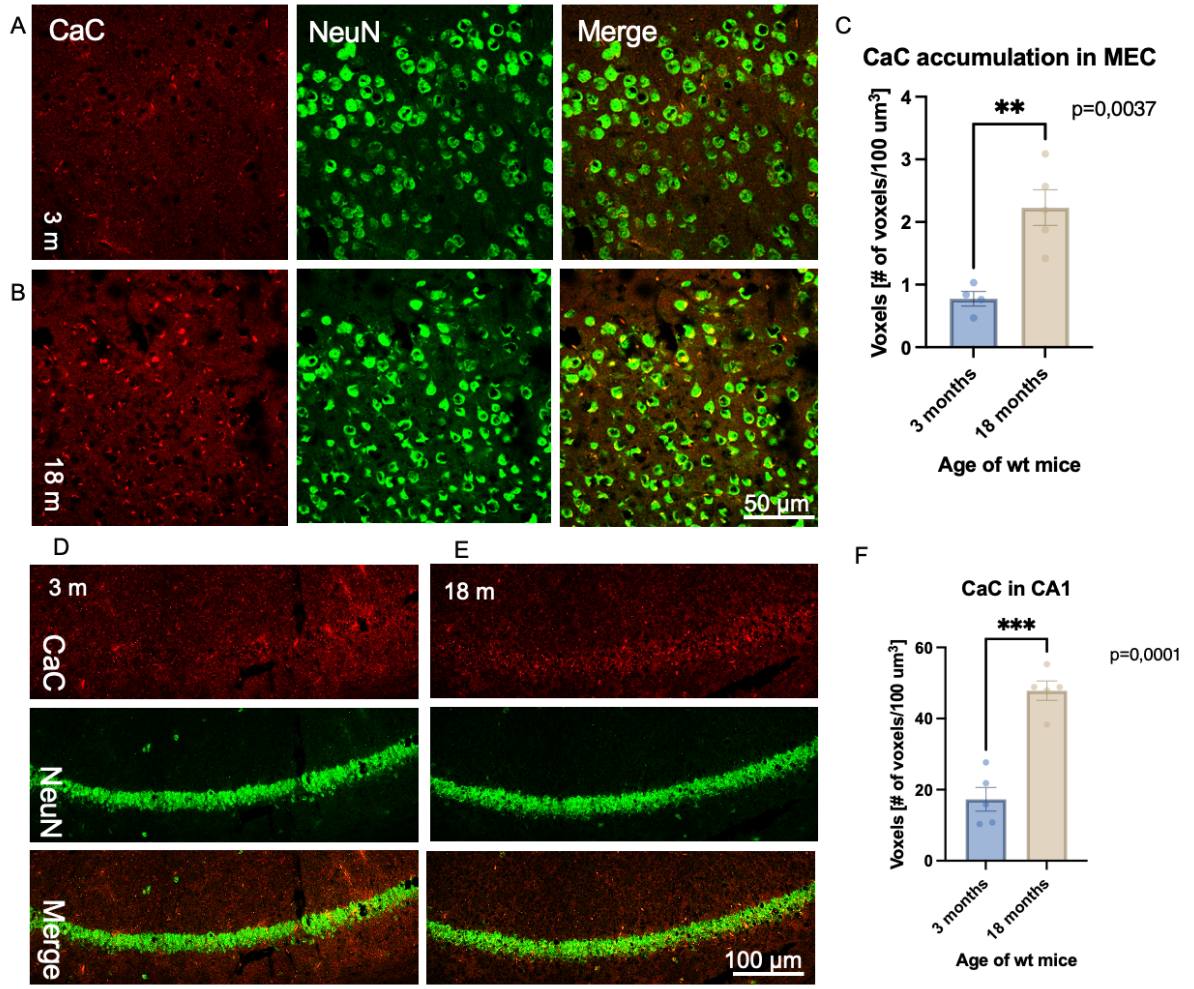

Figure 8 5CaC levels in young and aged MEC and CA1 A/B) Immunofluorescent staining of 5CaC in the MEC. *5CaC signal (red) is detected in MEC in young (3 m) mice but the signal is stronger in aged (18 m) mice. NeuN-staining (green) presents neurons in the MEC cell layers II and III. Scalebar 50 µm.* ***C) The histogram shows the level of 5CaC in young and aged MEC (total n=9).*** *A significant difference in 5CaC levels was detected comparing young and aged mice in MEC (Statistically significant; unpaired t-test, p-value <0.05).* ***D/E) Immunofluorescent staining of 5CaC in the hippocampal CA1.*** *5CaC signal (red) is detected in the pyramidal layer of CA1 in young (3 m) mice but the signal is stronger in aged (18 m) mice. NeuN-staining (green) presents neurons of the pyramidal cell layer in CA1. Scalebar 100 µm* ***F) The histogram shows the level of 5CaC in CA1 neurons in the two groups age groups (total n=10).*** *A statistical difference in 5CaC levels was detected comparing young and aged mice in CA1 (Statistically significant; unpaired t-test, p-value <0.05).*

3.2 Assessing rAAV-Cre induced TDG-depletion in the hippocampal region

3.2.1 Assessing the infection efficiency of rAAV-Cre by GFP expression

I immunohistochemically stained brain tissue from *LoxP-MiniTdg*$^{+/+}$ mice (3 to 6 months) after rAAV-Cre-injections with anti-GFP (green fluorescent protein) to assess the viral infection efficiency. GFP functions as a gene reporter, as the *miniTdg*-mice has a stop codon located between two *loxP* sites upstream of the GFP gene (Figure 4) [30]. The gene is expressed if the floxed stop codon is removed by rAAV-SYN-Cre induced excision, making it possible to visualize Cre-induced TDG-depletion. I also used anti-NeuN as a neurological marker, as it is neural nuclei specific, and can be used to assess neuronal health [96]. In the first virus injection trials (1:5 in PBS), NeuN expression showed severe neuronal loss around the injection site (e.g., CA3 in TDG_247 and CA1 in TDG_248, Figure 9). Cre-induced GFP expression was detected in the same regions. In the viral injections with a 1:10 dilution, a similar pattern was detected, where NeuN expression showed severe neuronal loss around the injection site along with Cre-induced GFP expression (e.g., CA1 in TDG_178, Figure 9). In the control virus (rAAV-Venus) injected animals, Cre-induced fluorescent signal was evenly distributed in the pyramidal and granular cell layer (e.g., CA3 and DG in TDG_356, Figures 11A and 11C, Section 3.2.2). The fluorescent signal was not GFP-expression, but a YFP protein (Venus) that may be visualized when applying the anti-GFP antibody. However, in PBS- and control virus (rAAV-Venus) injected animals, no hippocampal lesions were detected by NeuN expression (Figures 10A and 11A in Section 3.2.2). These observations suggest that massive Cre expression causes neuronal loss and tissue lesions and that it is not caused by surgery procedures or virus administration. Several viral dilutions were tested to improve the efficiency of rAAV-Cre infection and to reduce neuronal loss. With a 1:20 viral dilution, no considerable lesions or neuronal loss was detected, and Cre-induced GFP expression was evenly distributed in cellular and granular cell layers of the hippocampus (e.g., CA1, CA3, and DG in TDG_399 and TDG_458, Figure 9). These results suggest that the most efficient viral infections are completed with a 1:20 dilution.

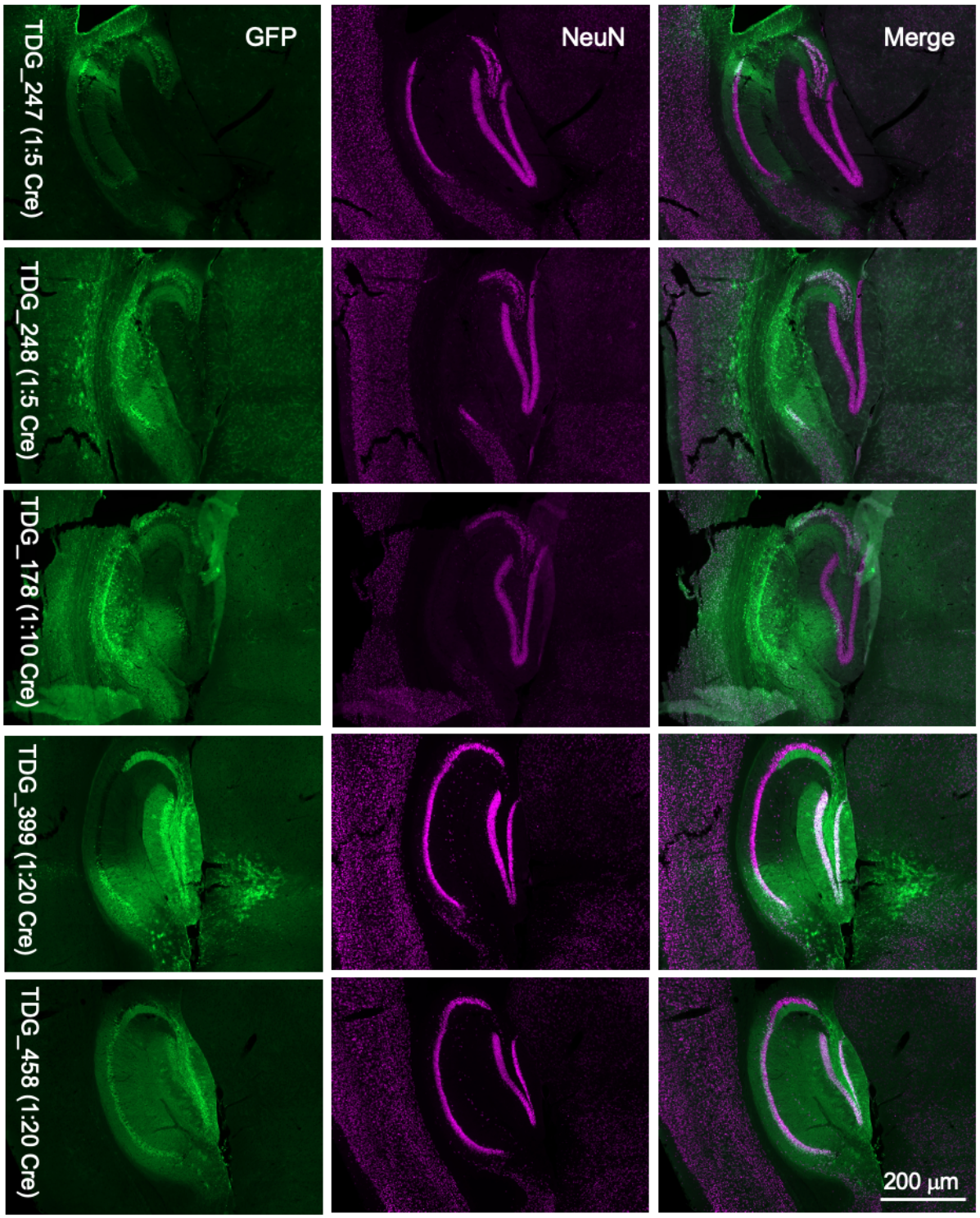

Figure 9. GFP and NeuN expression in mouse HPC after rAAV-Cre injection. *With 1:5 (TDG_247 and TDG_248) and 1:10 (TDG_178) dilutions, Cre-induced GFP expression was detected in hippocampal CA1 and CA3. NeuN expression showed neuronal loss in CA1 and CA3. With 1:20 dilution (TDG_399 and TDG_458), Cre-induced GFP expression was detected in the pyramidal (CA1/CA3) and granular (DG) cell layers. NeuN expression showed no neuronal loss. Scalebar 200 µm. Virus administration completed by Dagny Døskeland.*

3.2.2 Assessing immune response in viral injected animals

In order to assess the possible immune response in viral (rAAV-Cre) injected animals, anti-GFAP antibody was applied to visualize GFAP positive astrocytes. Astrocytes are found abundantly in the central nervous system (CNS) in a quiescent state as support cells of neural function [97, 98]. However, astrocytes have also been observed in association with CNS inflammation, where they are activated by injury and trauma [97]. When activated, the astrocytes become hypertrophic and the molecular expression changes. The changes are seen through upregulation of intermediate filament proteins, such as glia fibrillary acidic protein (GFAP) [99-101]. As cell mass and GFAP-levels increase in correlation with inflammation, anti-GFAP can operate as an immune response marker. No immune response was detected in control virus (rAAV-Venus) injected mice (e.g., TDG_356, Figure 11C), or naïve mice (e.g., TDG_275, Figure 12, B1), as only quiescent astrocytes were observed. However, activated GFAP-positive astrocytes were detected in the pyramidal and granular cell layers of the hippocampus (CA1, CA3, and DG) and around the injection site in rAAV-Cre injected mice (e.g., TDG_360, 1:5 dilution, Figure 11D; TDG_312, 1:5 dilution, Figure 12, B2). Strikingly, a distinct pattern of GFP expression was also detected in activated astrocytes around the injection site around the hippocampal cell layers (CA1, CA3, and DG, Figures 10B-D), further indicating an immune response. The observations suggest that the immune response is caused by rAAV-Cre infection, and not injections in general.

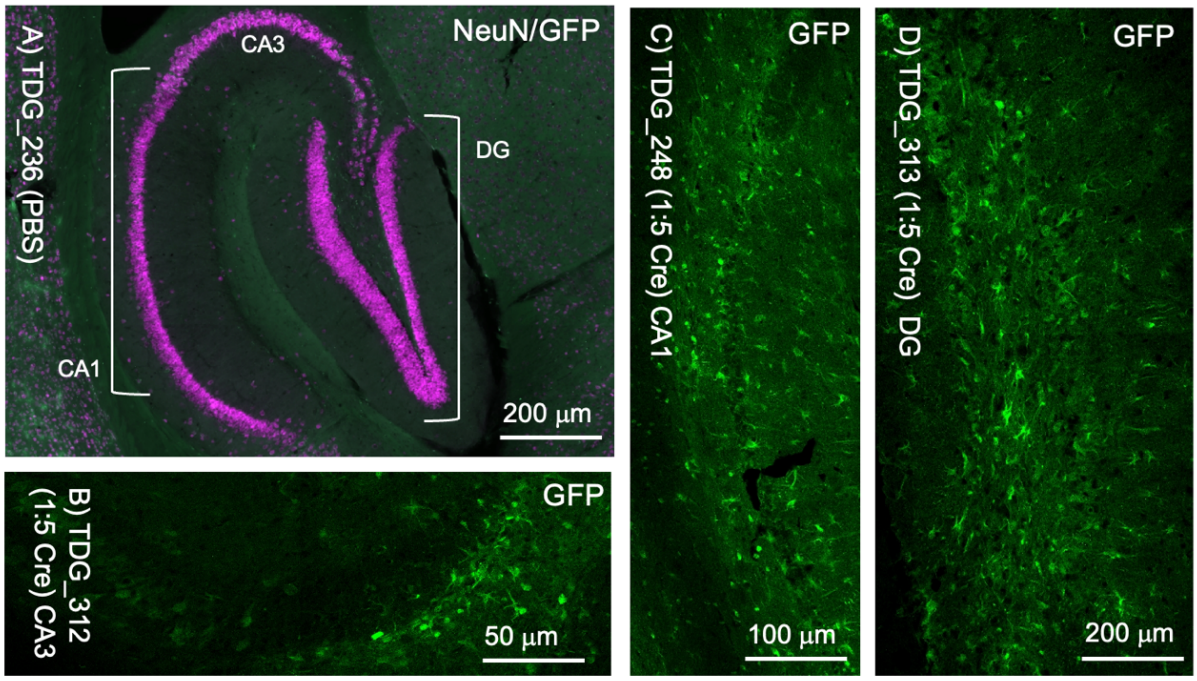

Figure 10 **Cre-induced GFP expression in activated hippocampal astrocytes. A) Representation of hippocampal regions (CA1, CA3, and DG) in PBS-injected mouse.** Anti-NeuN (magenta) and anti-GFP (green) staining. Scalebar 200 µm. **C-E) Cre-induced GFP expression in pyramidal and granular cell layer of 1:5 virus injected animals.** Cre-induced GFP expression (green) detected in activated astrocytes in hippocampal CA3, CA1, and DG. Scalebars 50, 100, and 200 µm. Virus administration completed by Dagny Døskeland.

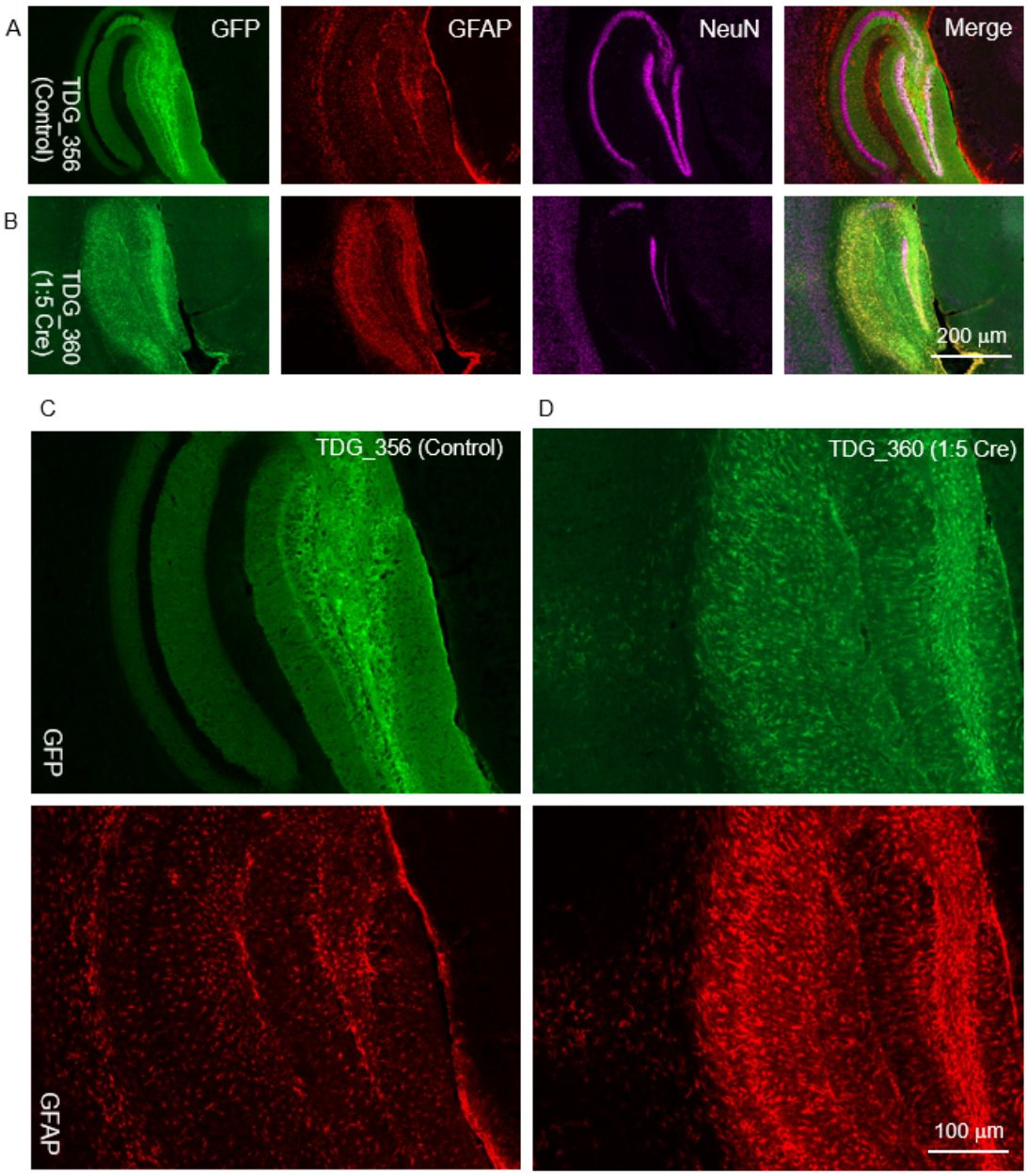

Figure 11 Hippocampal GFP- and GFAP expression A) Immunofluorescent staining of Cre-induced GFP fluorescent signal, GFAP-positive astrocytes, and surrounding neurons (NeuN) in control virus (rAAV-Venus) injected hippocampus*. Cre-induced GFP fluorescent signal (green) was evenly distributed in hippocampus. Quiescent GFAP-positive astrocytes (red) were detected in the hippocampus (See close-up* ***Figure 10C,*** *Scalebar 100 µm). NeuN expression (magenta) showed a healthy neuronal cell layer. Scalebar 200 µm.* ***B) Immunofluorescent staining of Cre-induced GFP expression, GFAP-positive astrocytes, and surrounding neurons (NeuN) in virus (1:5 rAAV-Cre) injected hippocampus****. Cre-induced GFP expression (green) was detected in the whole hippocampus in activated astrocytes and activated GFAP-positive astrocytes (red) were detected in the whole hippocampus (See close-up* ***Figure 10D****, Scalebar 100 µm). NeuN fluorescent expression (magenta) showed neuronal lesion the pyramidal layer, CA1 and partly CA3. Scalebar 200 µm. Virus administration completed by Dagny Døskeland.*

Immune response was also assessed through detection of activated microglia, using IHC with anti-Iba1 markers. Microglia are considered the principal macrophages in the CNS, which migrates to injured areas and consume cellular debris [102-104]. Therefore, anti-Iba1 functions as a sufficient immune response marker [105]. In rAAV-Cre (1:5) injected animals, Iba1-positive activated microglia were detected around the injection site (e.g., TDG_312, Figure 12, B4). In naïve animals, only Iba1-positive quiescent microglia were detected (e.g., TDG_276, Figure 12, B3). Again, the observations suggest that the rAAV-Cre-infection cause the immune response and the hippocampal lesions, and not the injections in general.

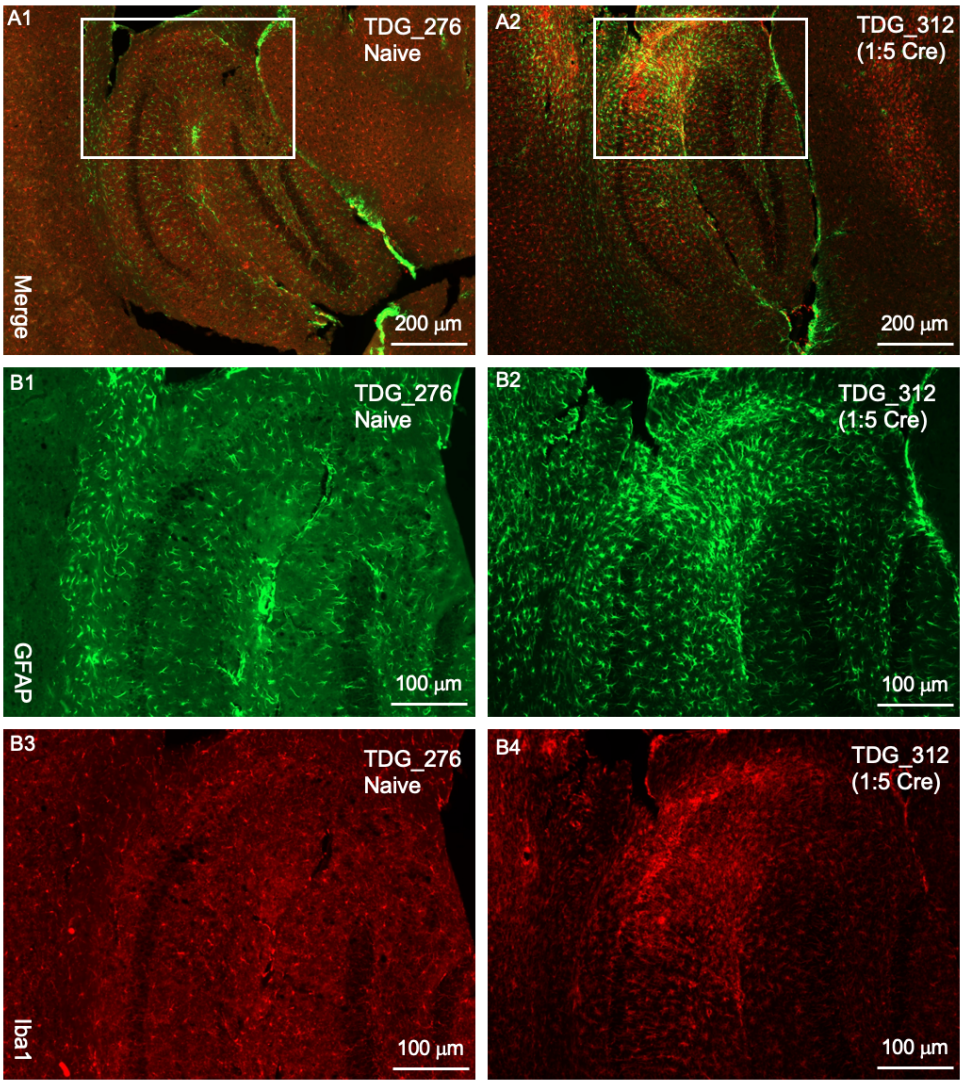

Figure 12 Hippocampal GFAP- and Iba1 expression A1-2) Full scale: Immunofluorescent staining of GFAP-positive astrocytes and Iba1-positive microglia in naïve and 1:5 rAAV-Cre injected mice. *Merged image of anti-GFAP (green) and anti-Iba1(red). White box present region in focus in Figure 12B1-4. Scalebar 200 µm.* ***B1-4) Zoomed in: Immunofluorescent staining of GFAP-positive astrocytes and Iba1-positive microglia in naïve and 1:5 rAAV-Cre injected mice.*** *Quiescent GFAP-positive astrocytes (green) and Iba1-positive microglia was detected in naïve hippocampus (TDG_276). Activated GFAP-positive astrocytes (green) were detected in the majority of hippocampus, especially at the injection site (CA1/CA3) in virus (1:5 rAAV-Cre) injected hippocampus (TDG_312). Iba1-positive microglia was detected at the injection site in the pyramidal cell layer of the hippocampus (partly CA1/CA3) in virus (1:5 rAAV-Cre) injected hippocampus (TDG_312). Scalebar 100 µm. Virus administration completed by Dagny Døskeland.*

3.2.3 Assessing rAAV-Cre induced TDG depletion by RT-qPCR

I performed a pilot experiment with RT-qPCR to assess rAAV-Cre induced TDG depletion in the hippocampus. RNA was extracted from hippocampal CA1, CA3, and DG from the left hemisphere of naïve (TDG_275) and 1:20 rAAV-Cre injected (TDG_400) animals. To minimize genomic DNA carryover, a DNase treatment was done before conduction cDNA synthesis. Primers (forward; reverse) applied for the RT-qPCR were *miniTdg*/TDG UTR, TDG exon 6/7, and mGAPDH_qPCR (Table 2, Section *2.4 RT-qPCR*). The TDG primers are different regions of the gene and display *Tdg* expression, while the GAPDH-primer functions as an internal control. GAPDH is a housekeeping gene and the expression levels are expected to remain constant when investigating tissues and cells [106]. The cycle threshold (CT) of GAPDH was used to normalize the CT values of the samples and to determine ΔCT values [ΔCT = sample (CT) – GAPDH (CT)]. ΔCT of naïve CA1, CA3, and DG, were selected as theoretical baselines. Naïve hippocampus is expected to have "normal" TDG expression, making their ΔCT values eligible to compare fold change (FC) in hippocampal TDG expression. Virus injected hippocampus are expected to have decreased TDG expression due to rAAV-Cre induced depletion. The theoretical baseline was used to determine ΔΔCT [ΔΔCT = sample (ΔCT) – baseline (ΔCT)], making it possible to calculate the FC [FC= 2^{-DDCT}]. The calculated FC shows reduced *miniTdg* expression in hippocampal DG and CA1, when comparing naïve and virus (1:20 rAAV-Cre) injected mice (Naïve TDG_275; 1:20 rAAV-Cre TDG_400, Figure 13B), suggesting Cre-induced TDG depletion. Unexpectedly, *miniTdg* expression in virus injected CA3 was 7-fold the expression in naïve CA3, probably indicating an error in the laboratory work. Reduced TDG exon expression was also observed in DG of virus injected hippocampus (1:20 rAAV-Cre TDG_400, Figure 13C) when compared to naïve hippocampus, indicating Cre-induced TDG depletion. Virus injected CA1 and CA3 showed and unexpected increase in FC of TDG exon compared to naïve CA1 and CA3, again, probably indicating an error in the laboratory work. IHC staining of hippocampus in the right hemisphere (e.g., TDG_399, Figure 13A) with anti-GFP shows Cre-induced GFP expression in the same regions as TDG levels were decreased compared to naïve animals, especially in DG where the highest FC was detected. The observations suggest that rAAV-Cre injections deplete TDG expression, but due to a limited amount of data and possible laboratory errors, the results are not reliable.

A

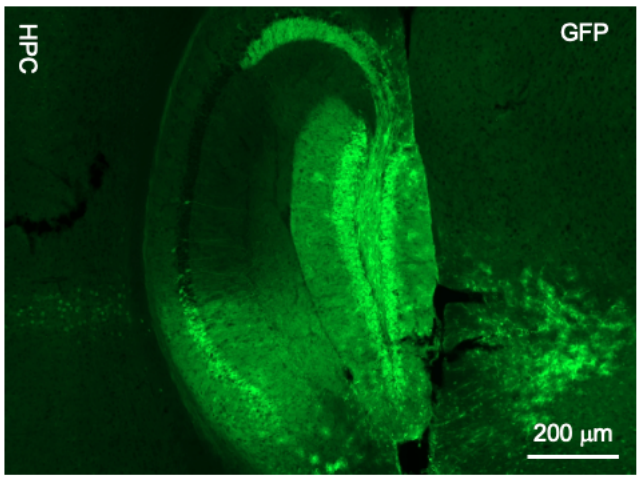

B

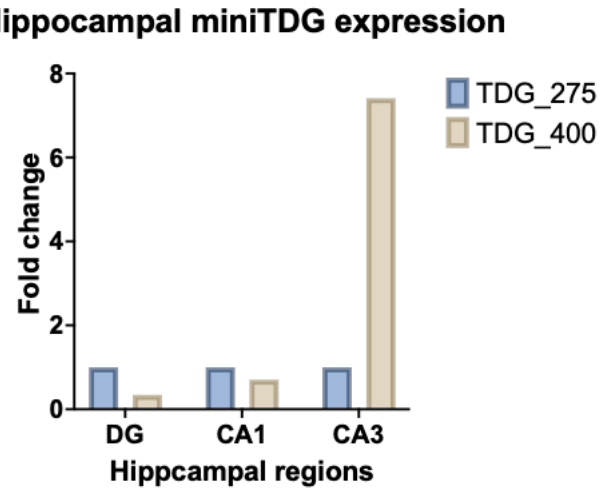

C

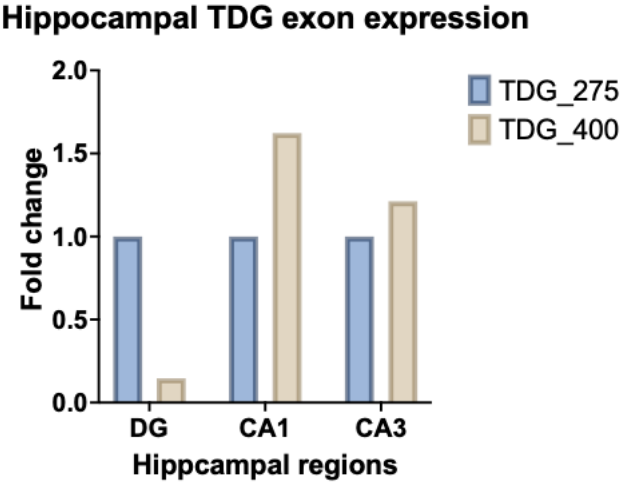

Figure 13 Hippocampal TDG-expression after rAAV-Cre injections A) Immunofluorescent staining of Cre-induced GFP expression in virus (1:20 rAAV-Cre) injected hippocampus (right hemisphere). *Cre-induced GFP expression (green) suggests TDG-depletion in pyramidal and granular cell layers of the hippocampus.* ***B) The histogram shows hippocampal miniTdg expression FC between naive and virus (1:20 rAAV-Cre) injected mice.*** *Hippocampal TDG expression compared between DG, CA1, and CA3 of naïve (TDG_275) and virus injected (TDG_400) animals. Normalized miniTdg FC (TDG_275: DG= 1; CA1= 1; CA3= 1).* ***C) The histogram shows hippocampal TDG exon expression FC between naïve and virus (1:20 rAAV-Cre) injected mice.*** *Hippocampal TDG expression compared between DG, CA1, and CA3 of naïve (TDG_275) and virus injected (TDG_400) animals. Normalized TDG exon FC (TDG_275: DG= 1; CA1= 1; CA3= 1). Virus administration completed by Dagny Døskeland.*

4. Discussion

4.1. Age-dependent regulation of DNA demethylation

The main aim with this project was to investigate the accumulation of DNA demethylation intermediates during aging. It is well known that both DNA methylation and demethylation are contributing immensely to cellular development and transcriptional regulation [92, 107-109]. This is among others seen through genomic imprinting, X-chromosome inactivation, and suppression of mobile genetic elements, as a result of 5mC-mediated gene silencing [110]. However, alterations in DNA methylation patterns during aging have also been observed and are referred to as the phenomenon of *epigenetic drift*. Epigenetic drift is when the methylomes of the elderly population differ from the younger populations, as the epigenetic resemblance decline over time [92]. Genome instability has been seen in association with aging and age-related pathologies, as a result of global genomic DNA hypomethylation [90, 91, 111]. On the other side, age-related DNA *hyper*methylation has been observed in association with gene suppression, in promoter regions [91, 92]. Most of the age-dependent alterations in methylation patterns have been found in studies based on whole blood genomic DNA and gives a picture of general cellular methylation patterns in the aging individual [92, 112]. The impact of altered DNA methylation patterns is not driven by whether methylation levels are increased or decreased, but rather age, tissue and genomic regions. Some epigenetic studies have also been conducted on brain tissue, such as the hippocampus, cerebellum, and cerebral cortex, in order to investigate the aging brain and brain pathologies, e.g., Alzheimer´s disease [53, 93-95]. Here, the DNA demethylation intermediate levels were studied in young (3 months) and aged mice (18 months), to investigate the age-dependent regulation of DNA demethylation.

4.1.1 Methodological considerations when investigating DNA demethylation during aging

In the investigation of DNA demethylation during aging, methodological strengths and weaknesses are found. The strength in this investigation is the sensitivity of immunohistochemistry (IHC), and the possibility to detect DNA demethylation intermediates by using specific epigenetic markers for 5hmC, 5fC, and 5CaC. Definite results are given within a relative short amount of time and the immunofluorescent signal is easy to detect through a confocal microscope. In addition, the images can easily be analyzed in 3D by IMARIS Cell imaging software.

However, some methodological weaknesses are also found in this investigation. Even though IHC is good way to detect specific immunofluorescent signal, the method is reliant on several factors, such as correct antigen retrieval buffer (pH), antibody specificity, and perfusion and tissue quality. The 30 µm thin brain sections can easily tear, making the wanted region insufficient for analysis. In general, IHC staining of epigenetic markers are highly achievable, but the findings would be strengthened by a supplementary procedure, e.g., Targeted Mass Spectrometry or epigenomic sequencing.

Another weakness found in the investigation considers the quantification of the immunofluorescent signal in IMARIS. In order to quantify the signals, a set threshold is used when obtaining the values (number of voxels; total volume) for the voxel ratio calculations (Calculation formula, *Section 2.7*). By setting a threshold, it is possible to statistically compare the voxel ratios to each other, as they are all based on the same conditions. However, brain tissue from the 3-month-old animals had relative low levels of DNA demethylation intermediates compared to 18-month-old animals. The low levels made the brain tissue more susceptible for contamination/noise in the form lines in the background, and corrections were done to make the voxel ratio as accurate as possible. For the young animals, a correction threshold was set to determine the number of voxels only based on the contamination signal. A corrected voxel ratio was then then determined by subtracting the correction number of voxels from the original number of voxels. The corrected voxel ratio might not be accurate, as too much signal might be removed by the correcting threshold. Due to time restraint, there was no time for re-staining and the source of the contamination was not found. The source of contamination is suspected to origin from microbial growth in the dilution buffer. In the future, a re-staining should be performed, and the dilution buffer should be kept in smaller aliquots or constantly in -20^{o}C.

The final weakness that should be taken into consideration is the number of animals being analyzed. Each age group consisted of 4-5 animals each (total n=10), which although makes it possible to perform statistical analysis, remains a low number of samples. In the future, a higher number of animals should be considered to gain a higher statistical power.

4.1.2 5hmC levels during aging in MEC and CA1

To investigate age dependent regulation of DNA demethylation, I performed immunohistochemical staining of MEC and hippocampal CA1 in young (3 months) and aged (18 months) WT mice with anti-5hmC. Literature and previous studies claim that 5hmC is seen abundantly in the nervous system and takes part in neuronal maturation and regulation of gene expression [42]. It is considered a stable epigenetic mark that is involved with regulation of genes associated to synapses and development [41-43]. 5hmC-levels have been seen increasing in different brain regions throughout life, particularly in neuronal differentiation [42, 44]. Most studies on 5hmC levels have been conducted on neuronal development, but there are a few that have been done during aging. Some studies show an increase in hippocampal 5hmC levels in aged mice [53, 54, 113], but other studies show a decrease in hippocampal 5hmC levels in aged mice [52, 95]. There might be reasons why the findings are divergent. Factors such as animal strain, age in the comparing groups, hippocampal regions, and methods used, might cause differences in the results. In the mentioned studies, all mice had the same background (C57BL6), but different strains were applied. IHC was used in most of the studies, but also different supplementary methods, e.g., ELISA and MeDIP. The research aims were also varying, with different factors such as physical exercise, caloric restriction and age-dependent Tet2-expression, which might drive the results in different directions. However, a similar molecular pattern should be observed, and further studies should be conducted.

In my investigation, 5hmC levels were increased in the MEC-layer II/III and in the pyramidal cell layer of CA1 in aged mice when compared to young mice (Figure 6, Section 3.1.1). However, the increased 5hmC levels were not statistically significant. The detection

of increased 5hmC levels in MEC and CA1 from the IHC staining correlates with some of the previous studies [53, 54, 113]. However, as no statistical difference was detected between young and aged animals, it would be biased to assume greater 5hmC levels in aged MEC and HPC neurons. By adding more animals to the investigation and adding supplementary methods, a more pronounced difference could be found.

4.1.3 Increased 5fC and 5CaC levels during aging in MEC and CA1

To investigate age dependent regulation of DNA demethylation, I also performed immunohistochemical staining of MEC and hippocampal CA1 in young (3 months) and aged (18 months) WT mice with anti-5fC and anti-5CaC. Studies on 5fC- and 5CaC levels in the entorhinal-spatial system during aging have not yet been conducted, but higher 5fC-levels have been observed in the aging cerebrum of human individuals [114]. Also, some studies have investigated the molecular function of the DNA demethylation intermediates (5fC and (5CaC), with results suggesting that 5fC is a stable DNA modification that can alter the DNA double helix structure [115, 116]. In addition, 5fC and 5CaC modifications might cause genome instability through transcriptional regulation and inhibit DNA replication [117, 118]. The characteristics of the 5fC and 5CaC make them interesting to investigate during aging in association with memory decline.

In my investigation, 5fC and 5CaC levels were increased in the aged MEC-layer II/III and in the CA1 pyramidal cell layer when compared to young mice. The increase was statistically significant (Figures 7/8, Sections 3.1.2 and 3.1.3). The result suggests that 5fC- and 5CaC levels accumulates in MEC and HPC neurons during aging, which correlates with the study performed on human cerebrum [114]. However, the mentioned study was mainly comparing 5fC levels in grey and white matter, and it was limited by the human brain tissue availability. Further studies must be done to get a better understanding of 5fC and 5CaC during aging. TDG recognize 5fC and 5CaC and excise them from the DNA strand in TDG-mediated active DNA demethylation, making TDG one of the main players in 5fC and 5CaC regulation [16, 17]. My results showing increased 5fC and 5CaC levels during aging, raises the question if TDG expression is age dependent or not. In the future, it would be interesting to investigate whether there are any association between accumulation of 5fC/5CaC levels and TDG reduction, in association with memory decline in aging.

4.2 Assessing rAAV-Cre induced TDG-depletion in the hippocampal region

The second aim of this project was to establish a reliable method for the conditional manipulation of TDG expression in neurons using the Cre-loxP system. Memory decline is seen in aging in association with epigenetic alterations, and the involvement of TDG is yet to be discovered. By creating TDG knockouts it might be possible in the future to evaluate the function of the gene and the impact it has on epigenetic regulation during aging. We can then further investigate if reduced TDG expression causes increased 5fC and 5CaC levels and epigenetic alterations. In order to evaluate the method, I assessed rAAV-Cre induced TDG-depletion in the hippocampal region of *LoxP-MiniTdg*$^{+/+}$ mice (3 to 6 months)

after viral injection. The assessment is based on infection efficiency through Cre-induced GFP expression, immune response, and molecular TDG-depletion by RT-qPCR.

4.2.1 Optimal infection efficiency with 1:20 rAAV-Cre injections

In order to assess the infection efficiency of rAAV-Cre injections, IHC was performed on 30 µm thin medial brain sections from *LoxP-MiniTdg*$^{+/+}$ mice (3 to 6 months) after virus (rAAV-Cre) and control virus (rAAV-Venus) injections (Figure 9, Section 3.2.1). Anti-GFP was used to visualize Cre-expression and to assess the infection range, while anti-NeuN was applied to assess neuronal health and possible loss. An efficient Cre-induced TDG depletion is crucial in research, as it is essential for the quality of the end results. For instance, if the purpose of the depletion is to study animal behavior after gene knockout, neuronal loss may interfere with the results. In addition, sever lesions may negatively impact animal welfare. Several viral dilutions were tested to improve the efficiency of rAAV-Cre infection and to reduce neuronal loss.

In the injection trials where dilutions of 1:5 and 1:10 rAAV-Cre viral stock were utilized, severe neuronal loss was detected in the pyramidal cell layer, with Cre-induced GFP expression in the same regions. When injecting dilutions of 1:20 rAAV-Cre viral stock, NeuN-expression showed no considerable lesions or neuronal loss, and Cre-induced GFP expression was evenly distributed in the pyramidal and granular cell layers. The results suggests that a 1:20 rAAV-Cre injection ensures the most efficient hippocampal TDG-depletion. Massive Cre expression seems to be linked to neuronal loss and tissue lesions, and a high viral concentration might cause more damage than good. These results are supported by control virus (rAAV-Venus) injections, where GFP fluorescent signal was also evenly distributed in the pyramidal and granular cell layers, yet no neuronal loss was detected. Furthermore, earlier trials with PBS-injected animals did not show any neuronal loss in the hippocampus either, suggesting that the lesions are not caused by the surgery procedure.

4.2.2 Massive Cre-expression activates immune response

The first GFP staining I performed on the brain tissue from *LoxP-MiniTdg*$^{+/+}$ mice (3 to 6 months), a rAAV-Cre viral stock with a dilution of 1:5 was injected. Both anti-GFP and anti-NeuN antibodies were used. Here, major hippocampal lesions were detected, along with Cre-induced GFP expression in astrocytes that first was suspected to be caused by contamination (Figure 10, Section 3.2.2). The observations led to a trouble shooting process, where the whole IHC procedure was systematically screened by reviewing all the steps and components involved (antibodies, blocking buffer, and dilution buffer). However, the Cre-induced GFP expression in the activated astrocytes was not caused by contamination but rather the result of an immune response. When microglia, the principal phagocytes of the central nervous system (CNS), are impaired by major lesions or aging, astrocytes are activated as a compensatory immune response mechanism [105, 119, 120]. Astrocytes are found abundantly in the CNS in a quiescent state, as support cells of neuronal function, until activation [97, 98]. Normally, microglia migrate to injured areas and consume cellular debris, a process that is important to avoid damaging the surrounding

neuronal tissue and contribute to neuronal development [102-104]. Here, the Cre-induced GFP expression was caused by cellular debris that had been accumulated by compensating astrocytes.

After confirming that the GFP fluorescent signal from the astrocytes was not caused by contamination but actual GFP expression, I initiated a new staining experiment with immune response markers. I used antibodies to detect the possible accumulation of Iba1 positive microglial cells and GFAP positive astrocytes (Figure 11/12, Section 3.2.2). When quiescent astrocytes are activated, they become hypertrophic and the molecular expression are altered through, e.g., upregulation of intermediate filament proteins such as glia fibrillary acidic protein (GFAP) [99-101]. Therefore, the GFAP antibody also functions as an adequate immune marker. In addition to Iba1 and GFAP antibodies, anti-NeuN was applied to investigate neuronal loss, especially in rAAV-Cre-injected mice.

In my investigation, I found that injection of rAAV-Cre viral stock with a dilution of 1:5 and 1:10 led to neuronal loss and an escalated activation of GFAP-positive astrocytes and Iba1-postitive microglia in the pyramidal and granular cell layers. Activated immune response was especially seen around the injection site. However, in control virus (rAAV-Venus) injected mice and naïve mice, only quiescent astrocytes and microglia was detected, indicating no immune response. In addition, no neuronal loss was detected. These findings suggest that the immune response detected is caused by the rAAV-Cre infections and not the injections in general. It is known from previous studies that a rAAV-injections can cause an immune response [121]. However, studies have also shown that rAAV-injections can cause minimal immune response, or that the immune response can be reduced when using correct rAAV-titers and by carefully choosing the anatomical injection site [122, 123]. This correlates with the findings from the previous section (Section 4.2.1), where no neuronal loss was detected in 1:20 rAAV-Cre injected animals in contrast to major neuronal loss in 1:5 and 1:10 rAAV-Cre injected animals.

4.2.3 rAAV-Cre induced TDG depletion by RT-qPCR

In order to assess rAAV-Cre induced TDG depletion after viral infection, I performed a pilot experiment with RT-qPCR, analyzing hippocampal CA1, CA3, and DG from the left hemisphere of naïve and 1:20 rAAV-Cre injected animals (Figure 13, Section 3.2.3). The primers, miniTdg/TDG UTR (1) and TDG exon 6/7 (2), were both applied to detect TDG levels. For internal control, a GAPDH primer (mGAPDH_qPCR) was applied. When using primer 1, my results showed a reduced TDG expression in hippocampal DG and CA1 in the 1:20 rAAV-Cre injected animal, when compared to the naïve animal. When using primer 2, reduced TDG expression was also detected in DG in 1:20 rAAV-Cre injected animal. IHC staining of the hippocampus (right hemisphere) with anti-GFP showed correlating Cre-induced GFP expression in rAAV-Cre injected animals, especially in DG. The results suggest a Cre-induced TDG depletion. Shockingly, when using primer 1, 7-fold TDG levels were detected in the rAAV-Cre injected CA3, when compared to naïve CA3. Increased TDG-levels were also detected in rAAV-Cre injected CA1 and CA3, when using primer 2. The results were unanticipated, because naïve animals have "normal" TDG levels, while rAAV-Cre injected animals are expected to have reduced TDG levels.

The reason for the inconsistency in the result might lie in strengths and weaknesses of the method. A strength in this experiment, is the two-step RT-qPCR method that consists of several advantages [124]. First, cDNA synthesis is performed to create a cDNA pool that can be used multiple times and stored for long periods. Second, amplification of the target and reference gene can be amplified from the same cDNA pool without multiplexing. Third, the reaction buffers and conditions are optimized and are possible to use for each reaction. Finally, the priming options are flexible.

There are also weaknesses with this experiment. First, the diverse results suggests that technical errors might have occurred. The two-step RT-qPCR involves many procedural steps, increasing the opportunity for DNA contamination. A DNase treatment was performed to avoid genomic carry over, but the increased TDG-levels in the Cre-injected animals might imply that some errors took place during the procedure. The unexpected values might also be caused by pipetting errors, but due to limited sample size this cannot be for certain.

Second, an essential consideration is the quality of the primers. The primer is very specific and small deviations in the primer sequence can have major impact on the transcription. If this is the case, the high TDG levels in the rAAV-Cre injected animal might be false positives. In the future, this could be confirmed by e.g., using Western Blot as a supplementary method.

The greatest weakness in this experiment, is the sample size with only one animal in each group. In the beginning, another rAAV-Cre injected animal was included, but it had some undetermined values and had to be excluded. RT-qPCR procedure was run two times to improve the undetermined value, but without any changes, indicating that there was not enough cDNA in the sample. Still, if the total number would have been 3 animals, the sample size would still be limited. More animals should be added in the future in order to draw a conclusion, and to achieve more statistical power.

5. Conclusion and future considerations

In this project I had two main aims. First, I investigated age dependent regulation of DNA demethylation in MEC and hippocampal CA1, where I compared DNA demethylation intermediate levels in 3- and 18-months old WT mice. 5hmC, 5fC, and 5CaC levels were increased in aging MEC and CA1 when compared to young, but the increase was only significant in 5fC and 5CaC levels. Accordingly, my work suggests that 5fC and 5CaC accumulates in the MEC and HPC neurons during aging. However, future studies should continue to investigate age dependent DNA demethylation in association with memory decline during aging, as few have been done by now. Future studies should also include other techniques, e.g., Targeted MS or epigenome sequencing. It would also be interesting to investigate whether there is an association between increased hippocampal 5fC/5CaC levels, memory decline, and TDG regulation during aging, as the DNA demethylation intermediates are excised by TDG-mediated DNA base excision repair (BER) pathway.

Second, rAAV-Cre induced TDG depletion in the hippocampal region of *LoxP-MiniTdg*$^{+/+}$ mice (3 to 6 months) was assessed, after rAAV-Cre injections performed by Dagny Døskeland. Our result suggested that a 1:20 rAAV-Cre injection ensures the most efficient TDG depletion in the hippocampal region. We learned that with a reduced rAAV-Cre concentration, neuronal loss and immune response are limited. A reliable TDG knockout model with the Cre-loxP system was established, creating opportunities for future studies of TDG regulation in general and during aging. Furthermore, our result makes it possible to investigate the association between aging, memory decline and TDG-regulation. However, much must be done in the future before a closer understanding is achieved. Lastly, the pilot study with RT-qPCR did not provide any reliable results due to a limited sample size. RT-qPCR is a very efficient method and should be used in future studies of hippocampal TDG-depletion.

5. References

1. Weinhold, B., *Epigenetics: the science of change.* Environ Health Perspect, 2006. **114**(3): p. A160-7.
2. Saw, G. and F.R. Tang, *Epigenetic Regulation of the Hippocampus, with Special Reference to Radiation Exposure.* Int J Mol Sci, 2020. **21**(24).
3. Creighton, S.D., et al., *Epigenetic Mechanisms of Learning and Memory: Implications for Aging.* International Journal of Molecular Sciences, 2020. **21**(18): p. 6918.
4. Morris, M. and L. Monteggia, *Role of DNA methylation and the DNA methyltransferases in learning and memory.* Dialogues in clinical neuroscience, 2014. **16**: p. 359-71.
5. Day, J.J. and J.D. Sweatt, *DNA methylation and memory formation.* Nature Neuroscience, 2010. **13**(11): p. 1319-1323.
6. Moore, L.D., T. Le, and G. Fan, *DNA Methylation and Its Basic Function.* Neuropsychopharmacology, 2013. **38**(1): p. 23-38.
7. Poon, C.H., L.S.R. Tse, and L.W. Lim, *DNA methylation in the pathology of Alzheimer's disease: from gene to cognition.* Annals of the New York Academy of Sciences, 2020. **1475**(1): p. 15-33.
8. Landgrave-Gómez, J., O. Mercado-Gómez, and R. Guevara-Guzmán, *Epigenetic mechanisms in neurological and neurodegenerative diseases.* Frontiers in Cellular Neuroscience, 2015. **9**.
9. Wang, J., et al., *Epigenetic mechanisms in Alzheimer's disease: Implications for pathogenesis and therapy.* Ageing Research Reviews, 2013. **12**(4): p. 1024-1041.
10. Neidhart, M., *DNA Methylation – Introduction*. 2016, Elsevier. p. 1-8.
11. Wu, X. and Y. Zhang, *TET-mediated active DNA demethylation: mechanism, function and beyond.* Nat Rev Genet, 2017. **18**(9): p. 517-534.
12. Zhang, L., et al., *Thymine DNA glycosylase specifically recognizes 5-carboxylcytosine-modified DNA.* Nature Chemical Biology, 2012. **8**(4): p. 328-330.
13. Shen, L. and Y. Zhang, *5-Hydroxymethylcytosine: generation, fate, and genomic distribution.* Curr Opin Cell Biol, 2013. **25**(3): p. 289-96.
14. Chahrour, M., et al., *MeCP2, a Key Contributor to Neurological Disease, Activates and Represses Transcription.* Science, 2008. **320**(5880): p. 1224-1229.
15. Maiti, A. and A.C. Drohat, *Thymine DNA Glycosylase Can Rapidly Excise 5-Formylcytosine and 5-Carboxylcytosine: POTENTIAL IMPLICATIONS FOR ACTIVE DEMETHYLATION OF CpG SITES*.* Journal of Biological Chemistry, 2011. **286**(41): p. 35334-35338.
16. Shen, L. and Y. Zhang, *5-Hydroxymethylcytosine: generation, fate, and genomic distribution.* Current opinion in cell biology, 2013. **25**(3): p. 289-296.
17. Wu, X. and Y. Zhang, *TET-mediated active DNA demethylation: mechanism, function and beyond.* Nature Reviews Genetics, 2017. **18**(9): p. 517-534.
18. Visnes, T., et al., *Targeting BER enzymes in cancer therapy.* DNA Repair, 2018. **71**: p. 118-126.
19. Hegde, M.L., T.K. Hazra, and S. Mitra, *Early steps in the DNA base excision/single-strand interruption repair pathway in mammalian cells.* Cell Research, 2008. **18**(1): p. 27-47.
20. Leandro, G.S., P. Sykora, and V.A. Bohr, *The impact of base excision DNA repair in age-related neurodegenerative diseases.* Mutation research, 2015. **776**: p. 31-39.

21. Krokan, H.E. and M. Bjørås, *Base excision repair.* Cold Spring Harbor perspectives in biology, 2013. **5**(4): p. a012583-a012583.
22. Cortázar, D., et al., *Embryonic lethal phenotype reveals a function of TDG in maintaining epigenetic stability.* Nature, 2011. **470**(7334): p. 419-423.
23. Neddermann, P., et al., *Cloning and Expression of Human G/T Mismatch-specific Thymine-DNA Glycosylase.* Journal of Biological Chemistry, 1996. **271**(22): p. 12767-12774.
24. Hashimoto, H., et al., *Excision of 5-hydroxymethyluracil and 5-carboxylcytosine by the thymine DNA glycosylase domain: its structural basis and implications for active DNA demethylation.* Nucleic Acids Research, 2012. **40**(20): p. 10203-10214.
25. Um, S., et al., *Retinoic Acid Receptors Interact Physically and Functionally with the T:G Mismatch-specific Thymine-DNA Glycosylase*.* Journal of Biological Chemistry, 1998. **273**(33): p. 20728-20736.
26. Chen, D., et al., *T:G Mismatch-specific Thymine-DNA Glycosylase Potentiates Transcription of Estrogen-regulated Genes through Direct Interaction with Estrogen Receptor α*.* Journal of Biological Chemistry, 2003. **278**(40): p. 38586-38592.
27. Li, Y.-Q., et al., *Association of Dnmt3a and thymine DNA glycosylase links DNA methylation with base-excision repair.* Nucleic Acids Research, 2007. **35**(2): p. 390-400.
28. Kim, H., et al., *Mouse Cre-LoxP system: general principles to determine tissue-specific roles of target genes.* Laboratory animal research, 2018. **34**(4): p. 147-159.
29. Sauer, B. and N. Henderson, *Site-specific DNA recombination in mammalian cells by the Cre recombinase of bacteriophage P1.* Proceedings of the National Academy of Sciences, 1988. **85**(14): p. 5166-5170.
30. Meinke, G., et al., *Cre Recombinase and Other Tyrosine Recombinases.* Chemical Reviews, 2016. **116**(20): p. 12785-12820.
31. Rajewsky, K., et al., *Conditional gene targeting.* Journal of Clinical Investigation, 1996. **98**(3): p. 600-603.
32. Kügler, S., E. Kilic, and M. Bähr, *Human synapsin 1 gene promoter confers highly neuron-specific long-term transgene expression from an adenoviral vector in the adult rat brain depending on the transduced area.* Gene Therapy, 2003. **10**(4): p. 337-347.
33. Leuner, B. and E. Gould, *Structural plasticity and hippocampal function.* Annual review of psychology, 2010. **61**: p. 111-C3.
34. Shors, T.J., *From stem cells to grandmother cells: how neurogenesis relates to learning and memory.* Cell Stem Cell, 2008. **3**(3): p. 253-8.
35. Halder, R., et al., *DNA methylation changes in plasticity genes accompany the formation and maintenance of memory.* Nature Neuroscience, 2016. **19**(1): p. 102-110.
36. Levenson, J.M., et al., *Evidence That DNA (Cytosine-5) Methyltransferase Regulates Synaptic Plasticity in the Hippocampus.* Journal of Biological Chemistry, 2006. **281**(23): p. 15763-15773.
37. Miller, C.A. and J.D. Sweatt, *Covalent Modification of DNA Regulates Memory Formation.* Neuron, 2007. **53**(6): p. 857-869.
38. Miller, C.A., et al., *Cortical DNA methylation maintains remote memory.* Nature Neuroscience, 2010. **13**(6): p. 664-666.

39. Liu, L., et al., *DNA methylation impacts on learning and memory in aging.* Neurobiology of aging, 2009. **30**(4): p. 549-560.
40. Zhou, F.C., et al., *Alcohol Alters DNA Methylation Patterns and Inhibits Neural Stem Cell Differentiation.* Alcoholism: Clinical and Experimental Research, 2011. **35**(4): p. 735-746.
41. Chen, Y., N.C. Ozturk, and F.C. Zhou, *DNA Methylation Program in Developing Hippocampus and Its Alteration by Alcohol.* PLoS ONE, 2013. **8**(3): p. e60503.
42. MacArthur, I.C. and M.M. Dawlaty, *TET Enzymes and 5-Hydroxymethylcytosine in Neural Progenitor Cell Biology and Neurodevelopment.* Frontiers in Cell and Developmental Biology, 2021. **9**.
43. He, B., et al., *Tissue-specific 5-hydroxymethylcytosine landscape of the human genome.* Nature Communications, 2021. **12**(1): p. 4249.
44. Hahn, M.A., et al., *Dynamics of 5-hydroxymethylcytosine and chromatin marks in Mammalian neurogenesis.* Cell reports, 2013. **3**(2): p. 291-300.
45. Zocher, S., et al., *Environmental enrichment preserves a young DNA methylation landscape in the aged mouse hippocampus.* Nature Communications, 2021. **12**(1): p. 3892.
46. Penner, M.R., et al., *Age-related changes inEgr1 transcription and DNA methylation within the hippocampus.* Hippocampus, 2016. **26**(8): p. 1008-1020.
47. Chouliaras, L., et al., *Consistent decrease in global DNA methylation and hydroxymethylation in the hippocampus of Alzheimer's disease patients.* Neurobiology of Aging, 2013. **34**(9): p. 2091-2099.
48. Christensen, B.C., et al., *Aging and Environmental Exposures Alter Tissue-Specific DNA Methylation Dependent upon CpG Island Context.* PLoS Genetics, 2009. **5**(8): p. e1000602.
49. López-Otín, C., et al., *The Hallmarks of Aging.* Cell, 2013. **153**(6): p. 1194-1217.
50. Horvath, S., *DNA methylation age of human tissues and cell types.* Genome Biology, 2013. **14**(10): p. R115.
51. Oliveira, A.M.M., T.J. Hemstedt, and H. Bading, *Rescue of aging-associated decline in Dnmt3a2 expression restores cognitive abilities.* Nature Neuroscience, 2012. **15**(8): p. 1111-1113.
52. Gontier, G., et al., *Tet2 Rescues Age-Related Regenerative Decline and Enhances Cognitive Function in the Adult Mouse Brain.* Cell Reports, 2018. **22**(8): p. 1974-1981.
53. Chen, H., S. Dzitoyeva, and H. Manev, *Effect of aging on 5-hydroxymethylcytosine in the mouse hippocampus.* Restorative Neurology and Neuroscience, 2012. **30**: p. 237-245.
54. Chouliaras, L., et al., *Age-Related Increase in Levels of 5-Hydroxymethylcytosine in Mouse Hippocampus is Prevented by Caloric Restriction.* Current Alzheimer Research, 2012. **9**(5): p. 536-544.
55. Feng, J., et al., *Dnmt1 and Dnmt3a maintain DNA methylation and regulate synaptic function in adult forebrain neurons.* Nature Neuroscience, 2010. **13**(4): p. 423-430.
56. Nelson, E.D., E.T. Kavalali, and L.M. Monteggia, *Activity-Dependent Suppression of Miniature Neurotransmission through the Regulation of DNA Methylation.* Journal of Neuroscience, 2008. **28**(2): p. 395-406.
57. Kaas, Garrett A., et al., *TET1 Controls CNS 5-Methylcytosine Hydroxylation, Active DNA Demethylation, Gene Transcription, and Memory Formation.* Neuron, 2013. **79**(6): p. 1086-1093.

58. Li, P., et al., *Epigenetic dysregulation of enhancers in neurons is associated with Alzheimer's disease pathology and cognitive symptoms.* Nature Communications, 2019. **10**(1): p. 2246.
59. Chouliaras, L., et al., *Epigenetic regulation in the pathophysiology of Alzheimer's disease.* Progress in Neurobiology, 2010. **90**(4): p. 498-510.
60. Mastroeni, D., et al., *Epigenetic changes in Alzheimer's disease: Decrements in DNA methylation.* Neurobiology of Aging, 2010. **31**(12): p. 2025-2037.
61. Coppieters, N., et al., *Global changes in DNA methylation and hydroxymethylation in Alzheimer's disease human brain.* Neurobiology of Aging, 2014. **35**(6): p. 1334-1344.
62. Anand, K.S. and V. Dhikav, *Hippocampus in health and disease: An overview.* Annals of Indian Academy of Neurology, 2012. **15**(4): p. 239-246.
63. *The Hippocampus Book*. Oxford Neuroscience Series. 2007, New York: Oxford University Press. 852.
64. GoodSmith, D., et al., *Spatial Representations of Granule Cells and Mossy Cells of the Dentate Gyrus.* Neuron, 2017. **93**(3): p. 677-690.e5.
65. Leutgeb Jill, K., et al., *Pattern Separation in the Dentate Gyrus and CA3 of the Hippocampus.* Science, 2007. **315**(5814): p. 961-966.
66. Nicoll, R.A., *A Brief History of Long-Term Potentiation.* Neuron, 2017. **93**(2): p. 281-290.
67. Baudry, M., *Long-term Potentiation (Hippocampus)*, in *International Encyclopedia of the Social & Behavioral Sciences*, N.J. Smelser and P.B. Baltes, Editors. 2001, Pergamon: Oxford. p. 9081-9083.
68. Sun, C., et al., *Hippocampal neurons represent events as transferable units of experience.* Nature Neuroscience, 2020. **23**(5): p. 651-663.
69. Derdikman, D. and E.I. Moser, *Chapter 4 - A Manifold of Spatial Maps in the Brain**Reprinted from Trends in Cognitive Sciences, Vol 14, Dori Derdikman, Edvard Moser, A manifold of spatial maps in the brain, pg 561–569, 2010, with permission from Elsevier*, in *Space, Time and Number in the Brain*, S. Dehaene and E.M. Brannon, Editors. 2011, Academic Press: San Diego. p. 41-57.
70. Deshmukh, S. and J. Knierim, *Representation of Non-Spatial and Spatial Information in the Lateral Entorhinal Cortex.* Frontiers in Behavioral Neuroscience, 2011. **5**.
71. Naber, P.A., et al., *Parallel input to the hippocampal memory system through peri- and postrhinal cortices.* Neuroreport, 1997. **8**(11): p. 2617-21.
72. Hafting, T., et al., *Microstructure of a spatial map in the entorhinal cortex.* Nature, 2005. **436**(7052): p. 801-806.
73. Savelli, F., D. Yoganarasimha, and J.J. Knierim, *Influence of boundary removal on the spatial representations of the medial entorhinal cortex.* Hippocampus, 2008. **18**(12): p. 1270-1282.
74. Solstad, T., et al., *Representation of Geometric Borders in the Entorhinal Cortex.* Science, 2008. **322**(5909): p. 1865-1868.
75. Nakazawa, K., et al., *Requirement for Hippocampal CA3 NMDA Receptors in Associative Memory Recall.* Science, 2002. **297**(5579): p. 211-218.
76. Rajmohan, V. and E. Mohandas, *The limbic system.* Indian journal of psychiatry, 2007. **49**(2): p. 132-139.
77. Garcia, A.D. and E.A. Buffalo, *Anatomy and Function of the Primate Entorhinal Cortex.* Annual Review of Vision Science, 2020. **6**(1): p. 411-432.

78. Witter, M.P., et al., *Architecture of the Entorhinal Cortex A Review of Entorhinal Anatomy in Rodents with Some Comparative Notes.* Frontiers in Systems Neuroscience, 2017. **11**.
79. Navarro Schröder, T., et al., *Functional topography of the human entorhinal cortex.* eLife, 2015. **4**.
80. Khan, U.A., et al., *Molecular drivers and cortical spread of lateral entorhinal cortex dysfunction in preclinical Alzheimer's disease.* Nature Neuroscience, 2014. **17**(2): p. 304-311.
81. Sargolini, F., et al., *Conjunctive Representation of Position, Direction, and Velocity in Entorhinal Cortex.* Science, 2006. **312**(5774): p. 758-762.
82. Winterer, J., et al., *Excitatory Microcircuits within Superficial Layers of the Medial Entorhinal Cortex.* Cell Reports, 2017. **19**(6): p. 1110-1116.
83. Rowland, D.C., et al., *Functional properties of stellate cells in medial entorhinal cortex layer II.* eLife, 2018. **7**.
84. Stranahan, A.M., J.R. Erion, and M. Wosiski-Kuhn, *Reelin signaling in development, maintenance, and plasticity of neural networks.* Ageing research reviews, 2013. **12**(3): p. 815-822.
85. Fuchs, Elke C., et al., *Local and Distant Input Controlling Excitation in Layer II of the Medial Entorhinal Cortex.* Neuron, 2016. **89**(1): p. 194-208.
86. Kitamura, T., et al., *Island Cells Control Temporal Association Memory.* Science, 2014. **343**(6173): p. 896-901.
87. Muller, J.F., F. Mascagni, and A.J. McDonald, *Cholinergic innervation of pyramidal cells and parvalbumin-immunoreactive interneurons in the rat basolateral amygdala.* The Journal of comparative neurology, 2011. **519**(4): p. 790-805.
88. Teipel, S.J., et al., *Cholinergic System Imaging in the Healthy Aging Process and Alzheimer Disease*, in *Encyclopedia of Neuroscience*, L.R. Squire, Editor. 2009, Academic Press: Oxford. p. 857-868.
89. Westerink, R.H., J.P. Beekwilder, and W.J. Wadman, *Differential alterations of synaptic plasticity in dentate gyrus and CA1 hippocampal area of Calbindin-D28K knockout mice.* Brain Res, 2012. **1450**: p. 1-10.
90. Heyn, H., et al., *Distinct DNA methylomes of newborns and centenarians.* Proceedings of the National Academy of Sciences, 2012. **109**(26): p. 10522-10527.
91. McClay, J.L., et al., *A methylome-wide study of aging using massively parallel sequencing of the methyl-CpG-enriched genomic fraction from blood in over 700 subjects.* Human Molecular Genetics, 2014. **23**(5): p. 1175-1185.
92. Zampieri, M., et al., *Reconfiguration of DNA methylation in aging.* Mechanisms of Ageing and Development, 2015. **151**: p. 60-70.
93. Siegmund, K.D., et al., *DNA Methylation in the Human Cerebral Cortex Is Dynamically Regulated throughout the Life Span and Involves Differentiated Neurons.* PLoS ONE, 2007. **2**(9): p. e895.
94. Chouliaras, L., et al., *Prevention of age-related changes in hippocampal levels of 5-methylcytidine by caloric restriction.* Neurobiology of Aging, 2012. **33**(8): p. 1672-1681.
95. Szulwach, K.E., et al., *5-hmC–mediated epigenetic dynamics during postnatal neurodevelopment and aging.* Nature Neuroscience, 2011. **14**(12): p. 1607-1616.
96. Gusel'nikova, V.V. and D.E. Korzhevskiy, *NeuN As a Neuronal Nuclear Antigen and Neuron Differentiation Marker.* Acta naturae, 2015. **7**(2): p. 42-47.
97. Placone, A.L., et al., *Human astrocytes develop physiological morphology and remain quiescent in a novel 3D matrix.* Biomaterials, 2015. **42**: p. 134-143.

98. Nash, B., K. Ioannidou, and S.C. Barnett, *Astrocyte phenotypes and their relationship to myelination.* Journal of anatomy, 2011. **219**(1): p. 44-52.
99. Sofroniew, M.V., *Molecular dissection of reactive astrogliosis and glial scar formation.* Trends in Neurosciences, 2009. **32**(12): p. 638-647.
100. Pekny, M. and M. Nilsson, *Astrocyte activation and reactive gliosis.* Glia, 2005. **50**(4): p. 427-434.
101. Giovannoni, F. and F.J. Quintana, *The Role of Astrocytes in CNS Inflammation.* Trends in immunology, 2020. **41**(9): p. 805-819.
102. Rigato, C., et al., *Pattern of invasion of the embryonic mouse spinal cord by microglial cells at the time of the onset of functional neuronal networks.* Glia, 2011. **59**(4): p. 675-695.
103. Sierra, A., et al., *Janus-faced microglia: beneficial and detrimental consequences of microglial phagocytosis.* Front Cell Neurosci, 2013. **7**: p. 6.
104. Tanaka, T., M. Ueno, and T. Yamashita, *Engulfment of Axon Debris by Microglia Requires p38 MAPK Activity*.* Journal of Biological Chemistry, 2009. **284**(32): p. 21626-21636.
105. Konishi, H., et al., *Astrocytic phagocytosis is a compensatory mechanism for microglial dysfunction.* The EMBO Journal, 2020. **39**(22).
106. Barber, R.D., et al., *GAPDH as a housekeeping gene: analysis of GAPDH mRNA expression in a panel of 72 human tissues.* Physiol Genomics, 2005. **21**(3): p. 389-95.
107. Veland, N. and T. Chen, *Chapter 2 - Mechanisms of DNA Methylation and Demethylation During Mammalian Development*, in *Handbook of Epigenetics (Second Edition)*, T.O. Tollefsbol, Editor. 2017, Academic Press. p. 11-24.
108. Johnson, A.A., et al., *The role of DNA methylation in aging, rejuvenation, and age-related disease.* Rejuvenation research, 2012. **15**(5): p. 483-494.
109. Zhou, F.C., *DNA methylation program during development.* Frontiers in biology, 2012. **7**(6): p. 485-494.
110. Kohli, R.M. and Y. Zhang, *TET enzymes, TDG and the dynamics of DNA demethylation.* Nature, 2013. **502**(7472): p. 472-479.
111. Liu, L., et al., *DNA methylation impacts on learning and memory in aging.* Neurobiol Aging, 2009. **30**(4): p. 549-60.
112. Boks, M.P., et al., *The Relationship of DNA Methylation with Age, Gender and Genotype in Twins and Healthy Controls.* PLOS ONE, 2009. **4**(8): p. e6767.
113. Jessop, P. and M. Toledo-Rodriguez, *Hippocampal TET1 and TET2 Expression and DNA Hydroxymethylation Are Affected by Physical Exercise in Aged Mice.* Frontiers in cell and developmental biology, 2018. **6**: p. 45-45.
114. Wagner, M., et al., *Age-dependent levels of 5-methyl-, 5-hydroxymethyl-, and 5-formylcytosine in human and mouse brain tissues.* Angewandte Chemie (International ed. in English), 2015. **54**(42): p. 12511-12514.
115. Raiber, E.-A., et al., *5-Formylcytosine alters the structure of the DNA double helix.* Nature structural & molecular biology, 2015. **22**(1): p. 44-49.
116. Bachman, M., et al., *5-Formylcytosine can be a stable DNA modification in mammals.* Nature Chemical Biology, 2015. **11**(8): p. 555-557.
117. Shibutani, T., et al., *Guanine- 5-carboxylcytosine base pairs mimic mismatches during DNA replication.* Scientific Reports, 2014. **4**(1): p. 5220.
118. Kellinger, M.W., et al., *5-formylcytosine and 5-carboxylcytosine reduce the rate and substrate specificity of RNA polymerase II transcription.* Nature Structural & Molecular Biology, 2012. **19**(8): p. 831-833.

119. Abiega, O., et al., *Neuronal Hyperactivity Disturbs ATP Microgradients, Impairs Microglial Motility, and Reduces Phagocytic Receptor Expression Triggering Apoptosis/Microglial Phagocytosis Uncoupling.* PLoS Biol, 2016. **14**(5): p. e1002466.
120. Pluvinage, J.V., et al., *CD22 blockade restores homeostatic microglial phagocytosis in ageing brains.* Nature, 2019. **568**(7751): p. 187-192.
121. Chu, W.S. and J. Ng, *Immunomodulation in Administration of rAAV: Preclinical and Clinical Adjuvant Pharmacotherapies.* Frontiers in Immunology, 2021. **12**.
122. Treleaven, C.M., et al., *Gene transfer to the CNS is efficacious in immune-primed mice harboring physiologically relevant titers of anti-AAV antibodies.* Molecular therapy : the journal of the American Society of Gene Therapy, 2012. **20**(9): p. 1713-1723.
123. Kaspar Brian, K., et al., *Adeno-associated virus effectively mediates conditional gene modification in the brain.* Proceedings of the National Academy of Sciences, 2002. **99**(4): p. 2320-2325.
124. Bustin, S.A., *A-Z of quantitative PCR*. 2004, La Jolla, CA: International University Line.

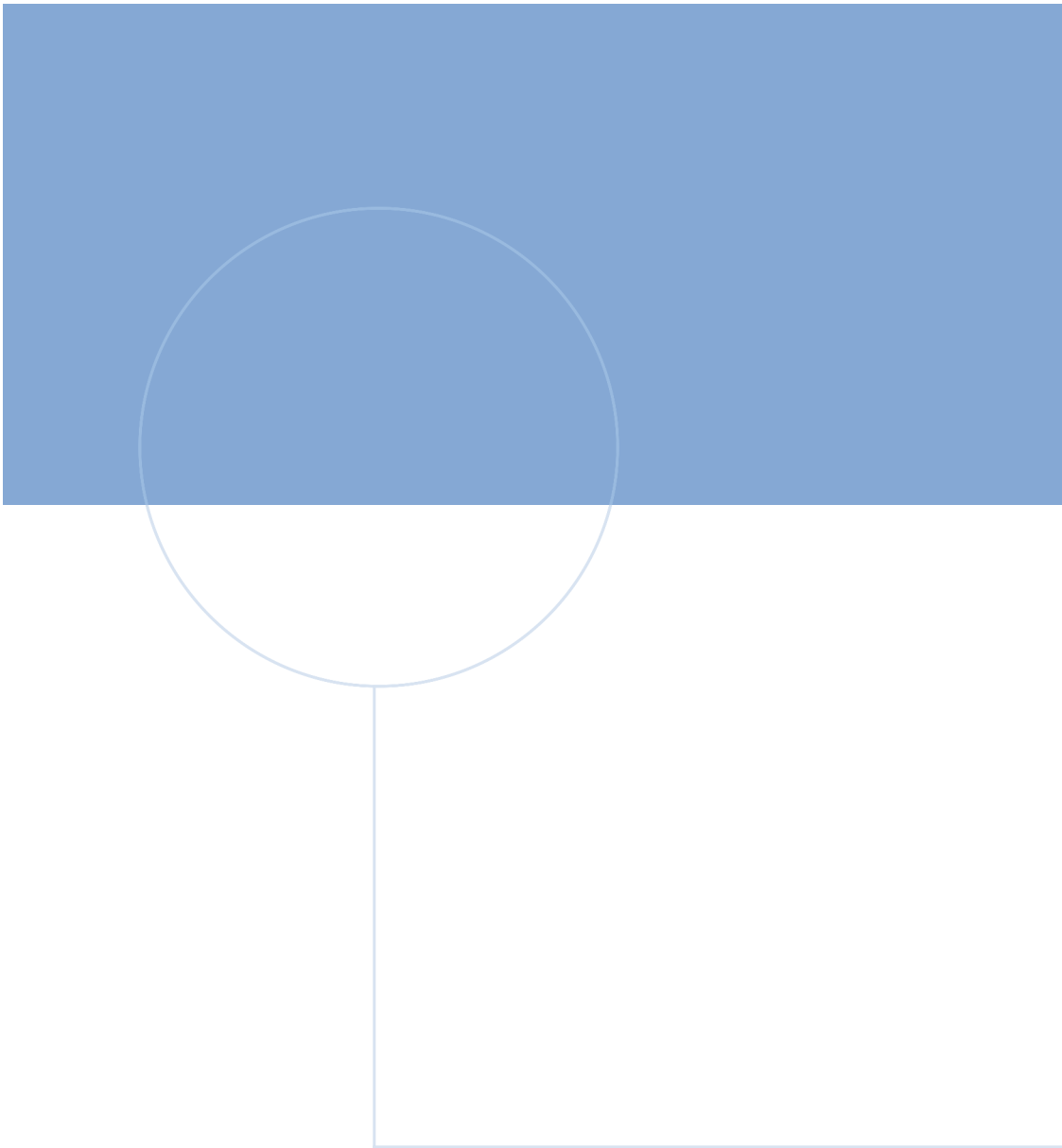

NTNU

Kunnskap for en bedre verden